The influence of magnetic fluctuations on collisional drift-wave turbulence

Suzana J. Camargo, Bruce D. Scott,[a] and Dieter Biskamp
Max-Planck-Institut für Plasmaphysik, EURATOM Association, 85748 Garching bei München, Germany

(Received 3 January 1996; accepted 19 July 1996)

A two-dimensional isothermal collisional drift-wave turbulence model including magnetic fluctuations is studied numerically. The model has as limits the electrostatic collisional drift-wave and two-dimensional magnetohydrodynamic systems. The electromagnetic and electrostatic regimes for thermal gradient-driven (drift-wave) turbulence are decided by the parameter $\hat{\beta}=(4\pi nT/B^2)(L_s^2/L_n^2)$, where L_s and L_n are the parallel and background profile scale lengths, respectively. Significant electromagnetic effects were found only for $\hat{\beta}\sim 10$ for most parameters, and were most pronounced in the strongly adiabatic regime for drift waves. The principal effect of the magnetic fluctuations is magnetic induction in the parallel force balance for electrons, which is linear. This diminishes the adiabaticity of the system by reducing the immediacy of the dissipative coupling between the density and electrostatic potential fluctuations. The transport was still found to be dominantly electrostatic even for $\hat{\beta}=10$, although its level decreased with $\hat{\beta}$ due to reduced coherency in the coupling between $E\times B$ velocity and density fluctuations. © *1996 American Institute of Physics.* [S1070-664X(96)00111-5]

I. INTRODUCTION

The physical processes of plasma transport in magnetic confinement devices, e.g., tokamaks, are not yet well understood. The transport of particles and energy is anomalous, i.e., the observed values are much larger than what is calculated by considering Coulomb collisions between the particles. It is usually assumed that the anomalous transport is due to the observed turbulent fluctuations of density, electric potential, and magnetic field. The presence of spatial plasma gradients in the plasma lead to collective oscillations called drift waves. The main effect of the drift-wave dynamics in the macroscopic scale is an anomalous diffusion of particles and energy along the corresponding gradient of the plasma density or temperature. Drift-wave turbulence is therefore considered as a possible cause for the anomalous transport in tokamaks.[1–3] Drift-wave turbulence theories are usually electrostatic, i.e., the fluctuations of the magnetic field are neglected.[3] However, it is not clear whether electrostatic or magnetic fluctuations (or both) are responsible for the anomalous transport.[4] Determining which fluctuation mechanism is dominant in driving the transport would provide a major constraint on the viability of various theories. An experimental determination of which effect is dominant would require a major advance in experiment diagnostics.[5]

Experimental measurements of the fluctuation of the magnetic field are difficult. Until recently only measurements of magnetic fluctuations at the plasma edge have been possible.[4] Even at the edge of the tokamak, it is difficult to make quantitative calculations of the effects of the magnetic fluctuations. Besides the coherent and high-beta magnetohydrodynamic (MHD) activities, such as sawteeth, fishbones, tearing modes, and edge localized modes (ELMs), broadband fluctuations are observed.[2] These incoherent magnetic fluctuations have amplitudes of $\delta B_\perp/B\sim 10^{-4}-10^{-5}$, with $\delta B_\perp \gg \delta B_\parallel$, are fairly isotropic perpendicular to **B**, and increase with decreasing minor radius.[1,2,4] Magnetic fluctuations have been considered a possible contributor for the transport in various tokamaks.[6] The magnetic fluctuations have been found both to correlate and not correlate with plasma transport in different machines. A correlation between the magnetic fluctuations and the quality of confinement is found during various transitions of confinement regimes (low-confinement or L-mode, high-confinement or H-mode, and ELMs).[2] The reversed field pinch (RFP) is ideal to study magnetic fluctuations as they are typically two orders of magnitude larger than those observed in tokamaks; theories can then be tested over a wider dynamic range than in tokamaks.[6–8] Recent experimental results for the RFP show that the magnetic fluctuations and the electrostatic fluctuations are related and conclude that suppressing the tearing mode activity could lead to a reduction of the edge electrostatic fluctuations.[9] By contrast, recent measurements in the Texas Experimental Tokamak (TEXT).[10] indicate that the magnetic fluctuations are not responsible for the transport of heat.[11] The fact that the level of magnetic fluctuations in the plasma boundary region is very small can lead to the conclusion that they do not play a significant role for transport,[12] even in the case of the RFP.[8] However, the issue cannot be assumed to be clear without a more complete investigation.

Many models have tried to relate the magnetic fluctuations to the transport in the plasma.[1,13–15] The theories have very different approaches to the problem. Typically these theories utilize quasilinear approximations and neglect self-consistent field effects. Some models calculate the anomalous electron thermal conduction due to the stochastic magnetic field, but without specifying the source of the magnetic fluctuations, e.g., Refs. 16 and 17. Other models consider, for instance, the anomalous electron thermal conductivity due to high-m ballooning modes.[18] Many studies of magnetic turbulence suppose a linear relation among the modes, relying on quasilinear or weak turbulence approaches or concentrate on the magnetic fluctuations associated with finite sized magnetic islands and microtearing modes.[14,19] MHD

[a]Electronic mail: bds@ipp-garching.mpg.de

 1070-664X/96/3(11)/3912/20/$10.00

turbulence,[20,21] which disregards the fluctuations of the density, was also studied thoroughly and has properties similar to fluid turbulence.

Although drift waves are basically electrostatic modes, they also have a small magnetic component, which can also lead to transport.[22] Magnetic fluctuations possibly associated with electromagnetic drift waves have been observed[23] in the edge of the Tokamak Chauffage Alfvén (TCA).[24] Quasilinear studies of electromagnetic drift waves have been performed by many authors, e.g., Ref. 1, and references therein. Calculations for stochastic diffusion of electrons in tokamaks due to a spectrum of electromagnetic drift fluctuations obtained diffusion coefficient scales approximating experimental scalings.[3] Other electromagnetic studies of drift-wave turbulence include the collisionless model of Molvig *et al.*[25] and the numerical simulations of Waltz.[26] A recent numerical study of a similar system with magnetic and density fluctuations, but disregarding potential fluctuations, observes three different turbulent states, even for identical parameters, making the turbulence state nonunique.[27] In Ref. 28 the anomalous transport due to electromagnetic drift-Alfvén turbulence was studied using DIA (direct interaction approximation) techniques, concluding that the electromagnetic contribution to transport by circulating electrons is important, while the transport dominated by trapped electrons is not affected by magnetic fluctuations. This result contrasts with another study of drift-Alfvén turbulence,[29] which concluded that electrostatic fluctuations alone regulate the transport. Another recent interesting analytical study of drift-wave theories, derived using a Lagrangian method, shows that the magnetic fluctuations may not be negligible even for $\beta \ll 1$.[30]

Three-dimensional numerical simulations of drift-wave turbulence confirm earlier indications that collisional drift-wave turbulence is the fundamental ingredient underlying tokamak edge and scrape-off layer turbulence.[31] It has also been suggested that edge turbulence could originate in the core plasma region,[32] where the magnetic fluctuations can be of fundamental importance. Experimental evidence of drift-wave-like instabilities in the core region of the tokamak is given in Ref. 33. Recent numerical simulations suggest the transition from resistive ballooning to drift-wave turbulence as a possible model for the transition between L- and H-mode confinement regimes.[34] Therefore, it is of fundamental importance to understand the role of the magnetic fluctuations in a simple drift-wave turbulence model, to better see how their effect should be considered in more realistic models.

The aim of this work is then to analyze the effect of the magnetic fluctuations in drift-wave dynamics. The magnetic fluctuations bring different physical effects into the system. We want to determine these effects and their role in the system. It is also important to understand whether the electrostatic approximation is a valid hypothesis when studying turbulence at the edge of the tokamak. We consider the magnetic fluctuations in a simple model for drift-wave turbulence. The properties of the Hasegawa–Wakatani system have been studied thoroughly in two and three dimensions.[35–40] This model is generalized by including the magnetic fluctuations in the equations. We then analyze how these fluctuations modify the properties of the electrostatic model. Related forms of these electromagnetic two-fluid equations were first derived independently by Hasegawa and Wakatani[41] and Hazeltine.[42] Also similar is the set of equations describing drift-tearing modes, both linearly[43] and nonlinearly,[44] and the parameters describing collisionality and electromagnetic character in that work carry over to the drift-wave system studied here. The model chosen has as its extreme limits the two-dimensional (2-D) Hasegawa–Wakatani model[35] and the 2-D MHD model,[20,21] both well known, which makes the interpretation of the results obtained easier. Bekki and Kaneda[45] performed low-resolution numerical simulations of this model in three dimensions, analyzing the formation of structures, but did not study the turbulent state. A related electromagnetic drift-wave system was studied numerically by Waltz.[26] A similar study has already been done for a more general set of equations,[46] but there numerical restrictions did not allow a thorough study of the electromagnetic effects. The numerical scheme employed here is similar to the one used for the Hasegawa–Wakatani model[36] and in other studies with a sheared magnetic field.[47]

The principal result of this study is that the role of the magnetic fluctuations is to reduce the immediacy of the coupling between the density and the electrostatic potential fluctuations in an otherwise electrostatic system. That is, the basic physics is that of drift waves with magnetic induction in the parallel electron force balance acting to enhance the nonadiabatic character of the turbulence by delaying the transient response between the density and electrostatic potential. These effects enter when the plasma beta reaches $\hat{\beta} \equiv (4\pi nT/B^2)(L_s^2/L_n^2) \sim 1$ and are really definitive when $\hat{\beta}$ is as high as 10 (the nominal regime boundary, which depends on simplified assumptions on the space and time scales, is $\hat{\beta} \sim 1$[48,49]). Even then, the transport is always nearly electrostatic. This result shows that the drift-wave part of a more complicated system can never be neglected, as shown previously in the case of rippling modes.[50] Specifically, microtearing[27] is unlikely to have any significant role on its own in anomalous transport in tokamaks.

In Sec. II the model and its main characteristics are described. The linear properties of the system are studied in Sec. III. Section IV describes the main results of the numerical simulations. In Sec. V, we study the linear mode interaction and the nonlinear transfer of energy, enstrophy, and magnetic potential. The conclusions are presented in Sec. VI.

II. MODEL AND INVARIANTS

The basic model employed in this study starts with the two-fluid collisional equations,[51] and then assuming the perpendicular velocities to be given by the $E \times B$ and diamagnetic drifts, the ions to be cold, and the temperature to be a constant. The latter two are done to elucidate the resulting dynamics by removing the complications of a finite ion gyroradius and thermal conduction. It is already known from both tearing-mode[44] and drift-wave[49] studies that the dynamics of the temperature and nonadiabatic portion of the density are qualitatively similar, even if quantitative differences are important. That is, the character of the system's internal dynamics, e.g., how nonadiabatic or electromagnetic it is, is the

same whether or not linear modes are stable, or whether or not a nonlinear instability is present. Since we are interested first in the qualitative question as to the conditions under which the system becomes electromagnetic, the role of the temperature gradient and fluctuations can be left to the near future.

A. Electromagnetic drift-wave equations

This model is a generalization of the Hasegawa–Wakatani system[41] in a shearless 2-D slab geometry when the magnetic fluctuations ψ are also considered. It can also be thought of as a restriction of the general fluid electron drift equations used in tearing-mode work,[43,44] to a homogeneous magnetic geometry (neglecting the parallel ion velocity). The total magnetic field **B** has a uniform component in the z direction, B_0, and the magnetic fluctuations ψ are in the plane (x,y):

$$\mathbf{B}=B_0\hat{e}_z-\nabla\times\psi\hat{e}_z. \tag{1}$$

Describing the dynamics in terms of nonlinear fluctuations, the electron density n is given by $n=n_0(1+n_1/n_0)$, with $n_1\ll n_0$. The equilibrium density $n_0(x)$ has a density gradient in the negative x direction, such that the equilibrium density scale $L_n=n_0/|dn_0/dx|$ is a constant.

We obtain the equations of the model from the Braginskii two-fluid equations;[51] the derivation is identical to that in the nonlinear tearing-mode studies.[44] Similar versions of the model were first obtained in Refs. 41 and 42, and an equivalent form can be found in Ref. 45. The drift-wave dispersion scale ρ_s and the sound speed c_s are defined, respectively, as $\rho_s = c\sqrt{M_iT}/eB$, $c_s = \sqrt{T/M_i}$, leading to the drift parameter $\delta_0=\rho_s/L_n$. The parallel scale length, which in this homogeneous setting replaces the shear length in the tearing-mode work, is L_s.

The fluctuations are scaled according to $\tilde{\phi}=(e\phi/T)\delta_0^{-1}$, $\tilde{n}=(n_1/n_0)\delta_0^{-1}$, $\tilde{\psi}=(\psi/B_0\rho_s)(L_s/L_n)\delta_0^{-1}$, and $\tilde{J}=(J_\parallel/nec_s)\times(L_n/L_s)\delta_0^{-1}$. Since $\tilde{J}$ is given by $\tilde{\psi}$, the set of dependent variables is given by $\{\tilde{\phi},\tilde{n},\tilde{\psi}\}$. The independent variables are scaled as $x\to x/\rho_s$, $y\to y/\rho_s$, $z\to z/L_s$, $t\to tc_s/L_n$.

The model equations are then given by

$$\frac{d_E}{dt}\tilde{\Omega}=\nabla_\parallel\tilde{J}, \tag{2}$$

$$\frac{d_E}{dt}\tilde{n}=-\frac{\partial\tilde{\phi}}{\partial y}+\nabla_\parallel\tilde{J}, \tag{3}$$

$$\frac{\partial\tilde{\psi}}{\partial t}=-\frac{\partial\tilde{\psi}}{\partial y}+\nabla_\parallel(\tilde{n}-\tilde{\phi})-D^{-1}\tilde{J}, \tag{4}$$

where

$$\tilde{\Omega}=\nabla_\perp^2\tilde{\phi}, \tag{5}$$

$$\tilde{J}=-\frac{1}{\hat{\beta}}\nabla_\perp^2\tilde{\psi}, \tag{6}$$

$$\frac{d_E}{dt}=\frac{\partial}{\partial t}+(\hat{\mathbf{z}}\times\nabla_\perp\tilde{\phi})\cdot\nabla_\perp, \tag{7}$$

$$\nabla_\parallel=\frac{\partial}{\partial z}-(\hat{\mathbf{z}}\times\nabla_\perp\tilde{\psi})\cdot\nabla_\perp, \tag{8}$$

$$\hat{\beta}=\frac{4\pi n_0T}{B_0^2}\frac{L_s^2}{L_n^2}, \tag{9}$$

$$D=\frac{c_s/L_n}{\nu_e}\frac{M_i}{m_e}\frac{L_n^2}{L_s^2}, \tag{10}$$

with $\partial/\partial z$ replaced in terms of a constant parallel wave number $K_\parallel=k_zL_s$ in Fourier space. The Fourier representation used is

$$f(x,y,z)\leftrightarrow\sum_{\mathbf{k}}f_{\mathbf{k}}e^{ik_xx+ik_yy+iK_\parallel z}, \tag{11}$$

where $\mathbf{k}=(k_x,k_y)$, noting again that there is only the one $K_\parallel$. For the nonlinear computations a dissipative correction to $\partial/\partial t$,

$$\frac{\partial}{\partial t}\to\frac{\partial}{\partial t}+\mu\nabla_\perp^4, \tag{12}$$

was added in each equation. These represent hyperviscosity-like terms and by taking appropriate values of μ confine the dissipation to the smallest scales resolved in the system.

The Hasegawa–Wakatani equations are obtained from Eqs. (2) to (4) by taking the limit $\tilde{\psi}\to0$ and $\tilde{J}=D(\partial/\partial z)(\tilde{n}-\tilde{\phi})$, which defines

$$\mathscr{C}=DK_\parallel^2 \tag{13}$$

as the nonadiabaticity parameter used earlier.[35,36] The adiabatic regime is, $\mathscr{C}\gg1$, such that the cross coupling forces $\tilde{n}$ to mimic $\tilde{\phi}$, which collects at the large scales.[36] The opposite limit, $\mathscr{C}\ll1$, is called the hydrodynamic regime, since the resulting freedom of $\tilde{n}$ results in its passive advection by the $E\times B$ velocity.[36] The 2-D MHD equations[20,21] can be obtained by taking constant density ($n=$constant) and $K_\parallel=0$. Hence, as noted and discussed first by Hazeltine,[42] this more inclusive set which can be called electromagnetic drift-wave equations, contains the dynamics of both the well-known 2-D Hasegawa–Wakatani and 2-D MHD systems.

It is apparent upon inspection of the model equations that the electromagnetic effects are controlled by $\hat{\beta}$. For $\hat{\beta}\ll1$ the current $\tilde{J}$ corresponds to weak magnetic fields $\tilde{\psi}$, such that the contribution of $\tilde{\psi}$ to the parallel gradient operator and the electromagnetic induction $(\partial\tilde{\psi}/\partial t)$ are negligible. We are therefore interested in studying the effect of large values of $\hat{\beta}$ in the model. We have essentially two free parameters once the appropriate normalization to L_s has been made ($K_\parallel=1$). These are D and $\hat{\beta}$—note that D is equivalent to $\mathscr{C}$, and henceforth will be cited as $\mathscr{C}$ except when deriving further equations. As the behavior for a fixed $\mathscr{C}$ is already known, it is interesting to take representative values for $\mathscr{C}$ corresponding to the adiabatic and hydrodynamic regimes, and then vary $\hat{\beta}$. The latter parameter determines the strength and influence of the magnetic fluctuations. A naive scaling based on linear drift-wave instabilities would assume a mode frequency, ω, and inverse scale, $k_\perp$, equal to unity in normalized units and then conclude that the electrostatic/electromagnetic regime boundary is $\hat{\beta}\sim1$, as in earlier

studies.[48,49] This is the point at which magnetic induction, $(\partial\tilde{\psi}/\partial t)$, would begin to overcome resistive dissipation, $\mathscr{C}^{-1}\tilde{J}$, for a nominal value of $\mathscr{C}\sim 1$. A better guess would therefore be that the system should become electromagnetic when $\hat{\beta}\mathscr{C}\sim 1$. Although the results we have obtained in the linear and turbulent regimes differ somewhat from this, it does explain why we found a more pronounced effect at higher $\mathscr{C}$: magnetic induction overcomes resistivity more easily at lower collisionality.

B. Invariants of the model

The invariants of the purely nonlinear subset of the electromagnetic drift-wave equations are the total fluctuation free energy (herein *energy*)

$$E=\frac{1}{2}\int d^2x\left(|\nabla_\perp\tilde{\phi}|^2+\tilde{n}^2+\frac{1}{\hat{\beta}}|\nabla_\perp\tilde{\psi}|^2\right)$$
$$=E^V+E^N+E^M, \tag{14}$$

the generalized enstrophy

$$U=\frac{1}{2}\int d^2x(\tilde{n}-\nabla_\perp^2\tilde{\phi})^2=\frac{1}{2}\int d^2x(\tilde{n}-\tilde{\Omega})^2, \tag{15}$$

and the magnetic potential

$$A=\frac{1}{2}\int d^2x\tilde{\psi}^2. \tag{16}$$

The energy was mentioned as an invariant of this model in Refs. 42 and 45, but the other two invariants were not considered. The Hasegawa–Wakatani system also has the total energy E (with $E^M=0$) and the generalized enstrophy U as invariants.[35,36] On the other hand, the 2-D MHD system has the total energy E (with $E^N=0$), the magnetic potential A, and the cross-helicity H as invariants[20,21] $(H=\int d^2x\mathbf{v}\cdot\mathbf{B}=\int d^2x\nabla_\perp\tilde{\phi}\cdot\nabla_\perp\tilde{\psi})$.

According to the electromagnetic drift-wave equations (2)–(4), the invariants, E, U, and A, evolve with time as

$$\frac{\partial E}{\partial t}=\Gamma_n-\Gamma_r-\mathscr{D}^E, \tag{17}$$

$$\frac{\partial U}{\partial t}=\Gamma_n-\mathscr{D}^U, \tag{18}$$

$$\frac{\partial A}{\partial t}=\Gamma_a-\Gamma_d-\mathscr{D}^A, \tag{19}$$

where

$$\Gamma_n=-\int d^2x\tilde{n}\frac{\partial\tilde{\phi}}{\partial y}, \tag{20}$$

$$\Gamma_r=D^{-1}\int d^2x\tilde{J}^2, \tag{21}$$

$$\Gamma_d=D^{-1}\int d^2x\tilde{\psi}\tilde{J}, \tag{22}$$

$$\Gamma_a=\frac{\partial}{\partial z}\int d^2x\tilde{\psi}(\tilde{n}-\tilde{\phi}), \tag{23}$$

$$\mathscr{D}^E=\mu\int d^2x(-\tilde{\phi}\nabla_\perp^4\tilde{\Omega}+\tilde{n}\nabla_\perp^4\tilde{n}+\tilde{J}\nabla_\perp^4\tilde{\psi}), \tag{24}$$

$$\mathscr{D}^U=\mu\int d^2x(\tilde{n}-\tilde{\Omega})\nabla_\perp^4(\tilde{n}-\tilde{Q}), \tag{25}$$

$$\mathscr{D}^A=\mu\int d^2x\tilde{\psi}\nabla_\perp^4\tilde{\psi}. \tag{26}$$

Γ_n, the source of energy, is the rate at which the energy is extracted from the density gradient. Γ_r is the rate at which the energy is resistively dissipated, and Γ_d the rate that the magnetic potential is resistively dissipated. Γ_a is the source of the magnetic potential, and is proportional to the nonadiabaticity of $\tilde{\phi}$ and $\tilde{n}$ (for $\tilde{n}=\tilde{\phi}$, $\Gamma_a=0$). The dissipation rates $\mathscr{D}^E$, $\mathscr{D}^U$, and $\mathscr{D}^A$ are due to the finite hyperviscosity added as described to Eqs. (2)–(4). For diagnostic purposes we also computed

$$P=\frac{1}{2}\int d^2x\tilde{\phi}^2 \tag{27}$$

from the results.

III. LINEAR ANALYSIS

This section contains brief analyses of the linear dispersion relation obtained from the model and the linear mode structure, here represented by the phase shifts exhibited among the dependent variables. The linear growth rates and phase shifts are useful in comparisons with the turbulent state in saturation, presented in Sec. IV.

A. Dispersion relation and growth rate

The linearized system is solved analytically, for which purpose the hyperviscosity, μ, is neglected. By linearizing and Fourier decomposing Eqs. (2)–(4) and assuming a modal dependence of the form $e^{i(\mathbf{k}\cdot\mathbf{x}-\omega t)}$, we obtain

$$\omega\tilde{\phi}_\mathbf{k}-K_\parallel(\tilde{\psi}_\mathbf{k}/\hat{\beta})=0, \tag{28}$$

$$\omega\tilde{n}_\mathbf{k}-k_y\tilde{\phi}_\mathbf{k}+k_\perp^2K_\parallel(\tilde{\psi}_\mathbf{k}/\hat{\beta})=0, \tag{29}$$

$$[\hat{\beta}(\omega-k_y)+iD^{-1}](\tilde{\psi}_\mathbf{k}/\hat{\beta})+K_\parallel(\tilde{\phi}_\mathbf{k}-\tilde{n}_\mathbf{k})=0. \tag{30}$$

The resulting dispersion relation may be cast as

$$\omega^2[\hat{\beta}D(\omega-k_y)+i]-DK_\parallel^2[\omega(1+k_\perp^2)-k_y]=0, \tag{31}$$

where once again $\mathscr{C}=DK_\parallel^2$ and since $K_\parallel=1$, D is $\mathscr{C}$.

One notes that if $\hat{\beta}\mathscr{C}$ is small and $\mathscr{C}$ is large then the bracketed expression in the second term vanishes. This recovers the familiar drift-wave dispersion curve in the adiabatic limit. Small corrections due to the finite $\mathscr{C}$ then give the basic collisional drift wave's growth rate. Another extreme is k_y and $k_\perp$ sufficiently small that $\omega^2\hat{\beta}-K_\parallel^2=0$. This of course recovers the Alfvén wave dispersion curve; in that limit there are only the two damped Alfvén waves and the mode at ''zero frequency'' which is the drift wave. Since the only free energy source considered is the thermal gradient (temperature times ∇n), only the drift-wave branch can correspond to an instability, and since this will tie the turbulence to the resulting small scales, the MHD regime will not be reached. Nevertheless, in general there are three linear modes

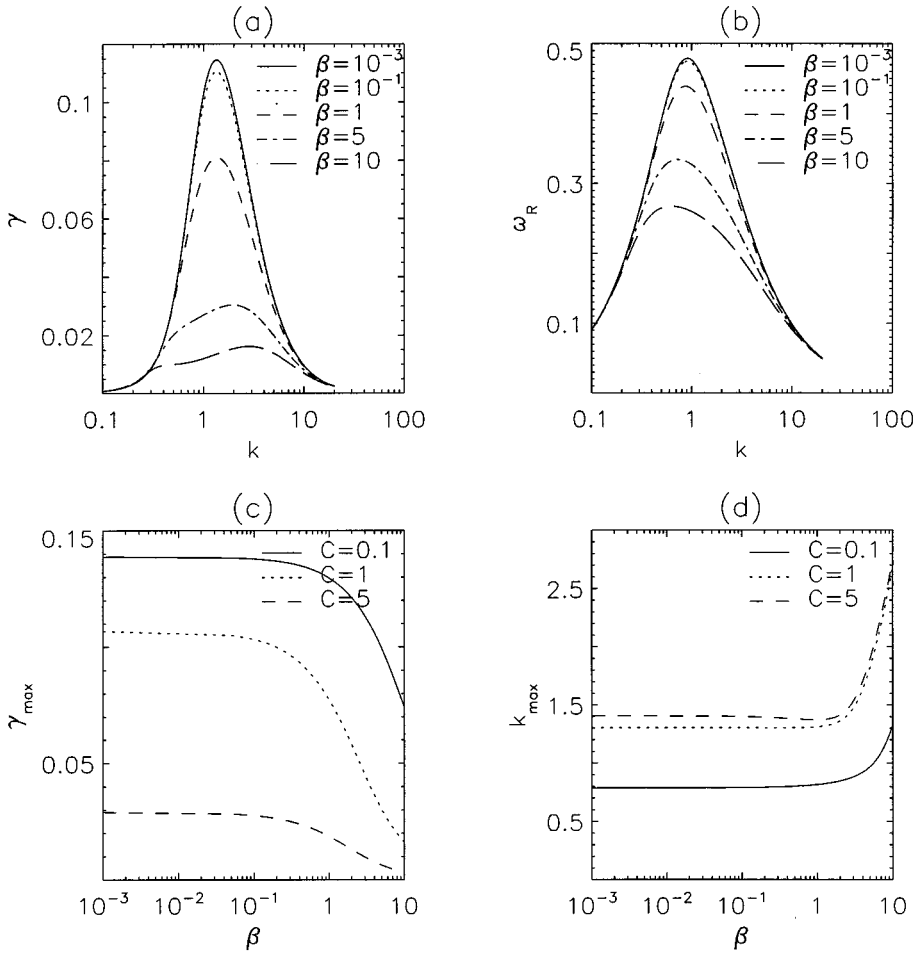

FIG. 1. The linear growth rate $\gamma(k)$ (a) and $\omega_R(k)$ (b) for $\mathscr{C}=1$ and different values of $\hat{\beta}$. The maximum of the linear growth rate $\gamma_{\max}$ (c) and the corresponding wave number $k_{\max}$ (d) as a function of $\hat{\beta}$ for $\mathscr{C}=0.1,1,5$.

in the system: one drift wave and two transients. The transients are resistively damped Alfvén waves, and it is worth noting that their behavior is quite different from the single dissipative transient in the electrostatic collisional drift-wave system. Rather than decaying at an unrealistically fast rate, the transients propagate back and forth along the field lines, decaying only at the rather slow rate, roughly $(\hat{\beta}\mathscr{C})^{-1}$. This is why magnetic induction begins to play a role in the dynamics as β increases and why it ultimately results in a more nonadiabatic character, as the latter is connected with the rate at which the transients damp.

The unstable mode corresponding to the drift wave is given by the single root of Eq. (31), which has a positive imaginary part. The mode frequency, $\omega_R(\mathbf{k})$, and linear growth rate, $\gamma(\mathbf{k})$, then follow.

In Fig. 1 we show the main properties of the linear growth rate, γ, and mode frequency, ω_R. The variation with different values of $\hat{\beta}$ for $K_\parallel=1$, $k_x=0$, $\mu=0$, and $\mathscr{C}=1$ is shown for both [Figs. 1(a) and 1(b)], and then the growth rate [Fig. 1(c)] and wave number [Fig. 1(d)] for the most unstable mode, k_y, is shown as a function of $\hat{\beta}$ for $\mathscr{C}=0.1$, 1, 5, and $k_x=0$, $K_\parallel=1$, $\mu=0$. One can see that for higher $\hat{\beta}$ the linear growth rate is smaller [Fig. 1(a)]. This decrease of $\gamma(\mathbf{k})$ with finite $\hat{\beta}$ is most pronounced in the adiabatic regime ($\mathscr{C}=5$), which also has smaller electrostatic growth rates [Fig. 1(c)]. When varying $\hat{\beta}$, the linear properties only have noticeable changes for $\hat{\beta}\gtrsim 1$ [Figs. 1(c) and 1(d)], confirming the naive estimate since the scaling of the most unstable mode's $k_\perp$ with $\mathscr{C}$ eliminates a strong dependence of the linear electromagnetic boundary on $\mathscr{C}$.

B. Linear phase shifts

The linear mode structure can be expressed in terms of the phase shifts among any two of the fluctuations in Fourier space, e.g., $\tilde{n}_{\mathbf{k}}$ and $\tilde{\phi}_{\mathbf{k}}$. From the linearized electromagnetic drift-wave equations (28)–(30), any two of the fluctuations can be computed from the third, given the result of the dispersion relation for the unstable mode. Since the ratio between any two complex numbers can be given in terms of an amplitude and a phase shift, the latter may be found from

$$\delta_{\mathbf{k}}=\mathrm{Im}\ \log\ \tilde{n}_{\mathbf{k}}^{*}\tilde{\phi}_{\mathbf{k}}, \tag{32}$$

$$\theta_{\mathbf{k}}=\mathrm{Im}\ \log\ \tilde{\phi}_{\mathbf{k}}^{*}\tilde{\psi}_{\mathbf{k}}, \tag{33}$$

$$\alpha_{\mathbf{k}}=\mathrm{Im}\ \log\ \tilde{n}_{\mathbf{k}}^{*}\tilde{\psi}_{\mathbf{k}}. \tag{34}$$

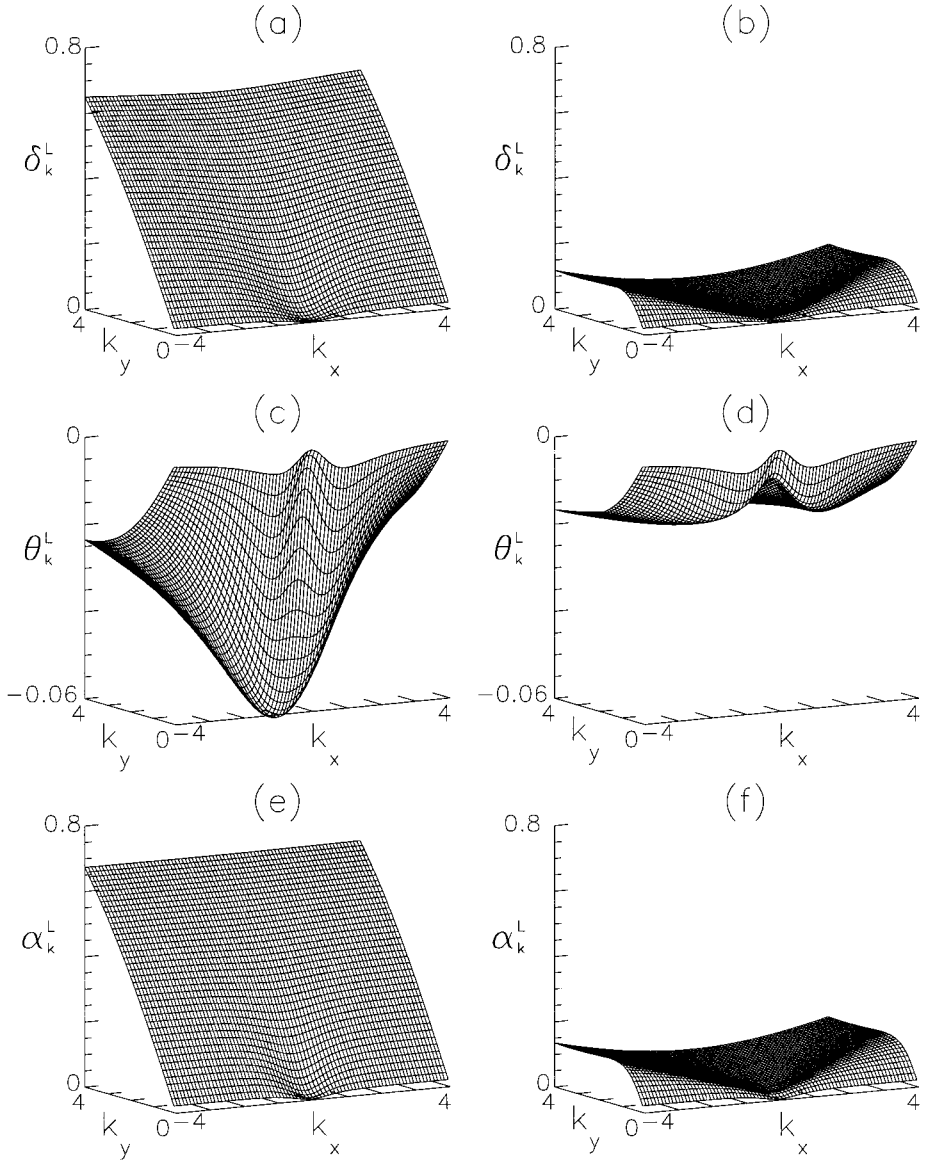

FIG. 2. Linear phase shifts for $\mathscr{C}=5$. δ_k^L for $\hat{\beta}=0.001$ (a) and $\hat{\beta}=10$ (b). θ_k^L for $\hat{\beta}=0.001$ (c) and $\hat{\beta}=10$ (d). α_k^L for $\hat{\beta}=0.001$ (e) and $\hat{\beta}=10$ (f).

Comparison to the nonlinear regime will be presented in Sec. IV using these same definitions. For the linear modes, the phase shifts satisfy:

$$\delta_{\mathbf{k}}^L = -\arctan\frac{k_y\gamma}{k^2(\omega_R^2+\gamma^2)-\omega_R k_y}, \tag{35}$$

$$\theta_{\mathbf{k}}^L = -\arctan\frac{\gamma}{\omega_R}, \tag{36}$$

$$\alpha_{\mathbf{k}}^L = -\arctan\frac{\gamma[k^2(\omega_R^2+\gamma^2)-2k_y\omega_R]}{k_y(\omega_R^2-\gamma^2)-k^2\omega_R(\omega_R^2+\gamma^2)}. \tag{37}$$

In Figs. 2(a) and 2(b) and $\delta_{\mathbf{k}}^L$ is shown for $\mathscr{C}=5$, with $\hat{\beta}=0.001$ and $\hat{\beta}=10$, respectively. Figures 2(c)–2(f) show $\theta_{\mathbf{k}}^L$ and $\alpha_{\mathbf{k}}^L$ for the same parameters. In this adiabatic limit the linear mode was most sensitive to $\hat{\beta}$ since it is easier for magnetic induction to overcome resistivity for low collisionality. For $\mathscr{C}=1$ the changes of the linear phase shifts for increasing values of $\hat{\beta}$ were still noticeable. In the hydrodynamic limit, the sensitivity of linear phase shifts to $\hat{\beta}$ was nearly absent, even at $\hat{\beta}=10$ at which $\hat{\beta}\mathscr{C}=1$, even though γ shows sensitivity at $\hat{\beta}=1$. This is a result of the already weak coupling of $\tilde{n}$ to $\tilde{\phi}$ for $\mathscr{C}<1$.

IV. COMPUTATIONS IN THE NONLINEAR REGIME

This section presents the computations which were performed and the essential results which describe the turbulent saturated state. In all cases, the property to look for is the strong effect of the increasing $\hat{\beta}$ in the adiabatic regime ($\mathscr{C}>1$), and the weaker effect in the hydrodynamic regime ($\mathscr{C}<1$). Especially important is the fact that the higher-$\hat{\beta}$, higher-$\mathscr{C}$ cases look qualitatively like the lower-$\mathscr{C}$ cases, that is, the principal effect of the electromagnetic character brought in by the finite $\hat{\beta}$ is to make the system appear more nonadiabatic. The reason is the magnetic induction, which

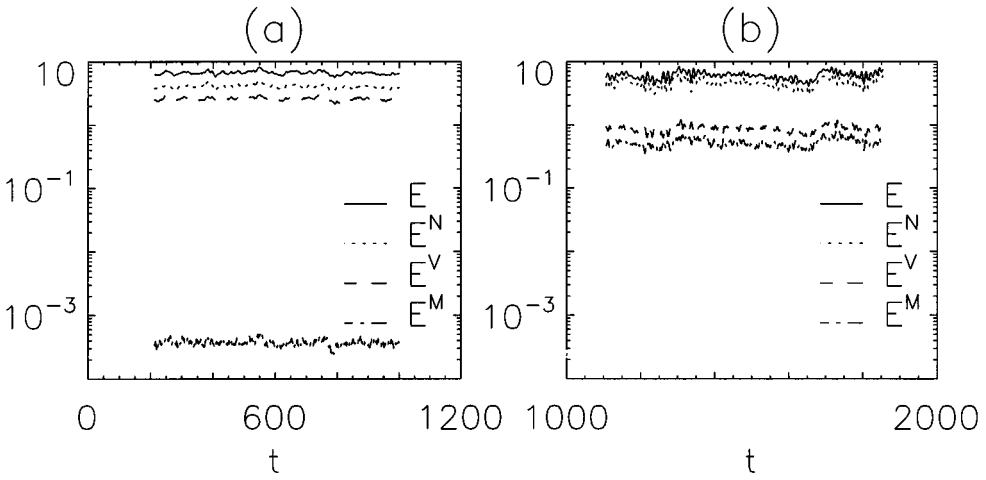

FIG. 3. The total energy E and the energy components E^N, E^V, E^M for $\hat{\beta}=0.001$ (a) and $\hat{\beta}=10$ (b) in the saturated state, with $\mathscr{C}=1$, $K_\parallel=1$, and $\mu=0.001$.

helps the density and electrostatic potential fluctuations to decouple much as does resistivity. Since the magnetic induction is a reactive (nondissipative) process, though, the coupling is not as coherent as when it is dissipative. Magnetic induction reduces both the immediacy and the coherence of the $\tilde{n}$-to-$\tilde{\phi}$ coupling, making it more difficult for free energy produced in $\tilde{n}$ by ∇n to return to $\tilde{\phi}$. It can be understood as a delay in the response of the electrons which is stabilizing to both linear waves and turbulence.

We find that the transition to the electromagnetic regime is definitive only for $\hat{\beta}=10$; the effect of magnetic induction $\hat{\beta}=1$ is still weak. In all cases, however, the electromagnetic corrections to $\nabla_\parallel$ are found to be sufficiently small that the transport caused by the turbulence is electrostatic.

A. Numerical details

The electromagnetic drift-wave equations (2)–(4) were solved on a square box of size $L^2=(2\pi/K_0)^2$ with periodic boundary conditions using a dealiased pseudospectral algorithm, similar to previous ones employed in studies of the Hasegawa–Wakatani system[36] and for a sheared magnetic field.[47] In most runs, the number of collocation points (grid nodes) was 128^2; in some cases a larger number (1024^2) was employed. The box size was chosen such that $K_0=0.15$. The dissipation parameter μ was taken to be just large enough to prevent numerical instability, $\mu=10^{-3}$ in most of the 128^2 runs. Another set of runs was considered to check for dependence on box size; for these we chose $K_0=0.0375$, $\mu\sim10^{-2}$, and in most cases 256^2 collocation points.

The method used to elucidate the role of electromagnetic effects and at which parameters they enter was to choose a reference value of $\mathscr{C}$ and then increase $\hat{\beta}$ from small values to large ones. In all cases, $K_\parallel$ was set to unity. Since the behavior of the system is known in the electrostatic limit (it is the Hasegawa–Wakatani system), the same three values used in our previous electrostatic work[36] were chosen: $\mathscr{C}=0.1$, 1, 5, representing a hydrodynamic, an intermediate, and an adiabatic regime, respectively. The electrostatic cases were reproduced by choosing $\hat{\beta}=10^{-3}$. Then, companion runs were done at $\beta=0.1$, 1.0, and 10.

The density $\tilde{n}$, potential $\tilde{\phi}$, and magnetic $\tilde{\psi}$ fluctuations were initialized with a random-phase, broadband field, such that all degrees of freedom are excited with a constant amplitude a_0

$$\sum_{\mathbf{k}} \tilde{\phi}_{\mathbf{k}}\tilde{\phi}_{\mathbf{k}}=\sum_{\mathbf{k}} \tilde{n}_{\mathbf{k}}\tilde{n}_{\mathbf{k}}=\sum_{\mathbf{k}} \tilde{\psi}_{\mathbf{k}}\tilde{\psi}_{\mathbf{k}}=a_0. \tag{38}$$

In most calculations, we chose $a_0=10^{-6}$, however in cases where the linear instability is very weak we considered $a_0=10^{-4}$, or even $a_0=10^{-2}$; so that the time required for reaching a turbulent saturated state would not be long. The numerical error was tracked in all runs using the energy equation (17); the numerical error was never greater than $0.01E$.

The runs with a finer grid (1024^2) were obtained by continuing the 128^2 runs and then increasing the number of collocation points to 256^2, 512^2, and finally 1024^2.

B. Properties of the saturated state

A typical numerical simulation has a linear phase, followed by a saturated turbulent state, which is then maintained long enough for good statistical quantities to be obtained.

In Figs. 3(a) and 3(b), the typical time evolution of the components of the energy E^N, E^V, and E^M for an electrostatic case ($\hat{\beta}=0.001$) and an electromagnetic case ($\hat{\beta}=10$) are shown. By analyzing Fig. 3, one can see that even for the case $\hat{\beta}=10$, the magnetic energy E^M is not the dominant component of the total energy E. By increasing $\hat{\beta}$, the role of the kinetic energy E^V diminishes in order to allow E^M to increase (see also Table I). In the hydrodynamic regime, the role of the density is so dominant, that the value of E^N/E is kept constant (0.83), independent of the value of $\hat{\beta}$. By contrast, in the adiabatic regime, the role of each component of

TABLE I. Saturation values in the different regimes. The electromagnetic component (A, E^M) enters with $\hat{\beta}$, and $\mathscr{C}=1$ is the most dissipative case.

$\mathscr{C}$	$\hat{\beta}$	E	E^N/E	E^V/E	E^M/E	U	A	P
	0.001	28.0	0.83	0.17	10^{-6}	42.1	10^{-6}	15.3
0.1	0.1	28.3	0.83	0.16	0.0006	42.3	0.009	16.1
0.1	10	13.1	0.83	0.14	0.03	18.8	20.1	8.7
	0.001	6.7	0.61	0.39	10^{-4}	14.0	10^{-7}	3.7
1	0.1	7.6	0.62	0.375	0.005	15.2	0.009	4.4
	10	6.0	0.77	0.14	0.09	7.3	30.1	6.2
	0.001	14.2	0.82	0.18	10^{-5}	18.4	10^{-6}	8.9
5	0.1	23.2	0.86	0.14	0.002	27.9	0.02	22.2
	10	4.4	0.78	0.13	0.09	5.1	13.8	3.7

the energy is much more affected by the values of $\hat{\beta}$. The saturation values of the total energy E, the enstrophy U, and amplitude P increase as $\hat{\beta}$ goes from 0.001 to 0.1 and diminish strongly for $\hat{\beta}=10$. The magnetic potential A saturation values increase with $\hat{\beta}$.

The spatial structure of the system is also altered by varying $\hat{\beta}$, which can be seen by analyzing the contour plots. Figures 4 and 5 show the typical contour plots of $\tilde{\phi}$, $\tilde{n}$, $\tilde{\psi}$, $\tilde{\Omega}$, and $\tilde{J}$ in the electrostatic and the electromagnetic regimes for $\mathscr{C}=5$. For each case, the contour plots were obtained at the same instant of time in a turbulent saturated state. In all contour plots, we considered $K_0=0.15$, $K_{\|}=1$, $\mu\sim 10^{-9}$ and 512^2 collocation points. Figures 4 and 5 show only the region $[0:\pi L]\times[0:\pi L]$, which is one-fourth of the real area calculated in the simulations. As usual, $\tilde{\phi}$ collects at large scales, owing to its inverse cascade tendency. With increasing $\hat{\beta}$ (Fig. 4), the resulting scale of $\tilde{\phi}$ is ever larger, since the reduction of the coupling between $\tilde{n}$ and $\tilde{\phi}$ allows the inverse cascade to evolve unhindered. This is also apparent in the difference between the electrostatic cases (see also Table III below). In the electromagnetic limit ($\hat{\beta}=10$), for $\mathscr{C}=5$, $\tilde{n}$ does not mimic $\tilde{\phi}$, but is more similar to $\tilde{\psi}$. The magnetic fluctuations $\tilde{\psi}$ have the same behavior in all regimes, always collecting in the larger scales. The vorticity $\tilde{\Omega}$ usually has fine structures; the presence of large $\hat{\beta}$ smooths these structures (Fig. 5). By contrast, the current $\tilde{J}$, which collects at average size structures in the electrostatic limit, shows a much finer structure in the electromagnetic limit. This effect, however, appears only in the adiabatic regime, in which the electromagnetic effects have a stronger influence.

The angle-averaged spectra of the invariants were also obtained (for the definition see Ref. 36). The spectra exhibit a maximum at a certain wave number k_{SM}. On the high-k side of the maximum k_{SM} there is an inertial range with a decaying power law spectrum (e.g., $E_k\sim k^{-a}$) up to the viscous cutoff. The variation of the spectral exponents with $\mathscr{C}$ and $\hat{\beta}$ is shown in Table II. In the electrostatic limit, the spectral exponents are almost identical to the Hasegawa–Wakatani case for $\mathscr{C}=0.1$ and $\mathscr{C}=1$.[36] However, for $\mathscr{C}=5$ the electromagnetic effects are stronger. Even for $\hat{\beta}=0.001$ in the adiabatic regime, the spectral exponents are higher than in the Hasegawa–Wakatani case. As $\hat{\beta}$ increases, the spectral exponents of the three invariants and the energy components increase for $\mathscr{C}=0.1$ and $\mathscr{C}=1$. In contrast, the spectral exponents of the energy E_k and its components (E_k^V, E_k^N and E_k^M) and the magnetic potential A_k diminish for $\mathscr{C}=5$, while the spectral exponents of the enstrophy increase. The spectral exponents for both the energy E_k and the magnetic potential A_k in the electromagnetic limit (independent of the value of $\mathscr{C}$) are very different from the ones obtained in 2-D MHD turbulence ($-3/2$ and $-7/3$, respectively[20]).

Figure 6 shows the variation of the spectra of energy components E_k^N, E_k^V, and E_k^M by varying $\hat{\beta}$. E_k^N, which is the dominant component of the energy, has a different behavior when $\hat{\beta}$ is increased for $\mathscr{C}=0.1$ and $\mathscr{C}=5$. E_k^V is not much affected by increasing $\hat{\beta}$, especially for $\mathscr{C}=0.1$. The magnetic energy component E_k^M also has a steeper curve in the electromagnetic regime ($\hat{\beta}=10$) than in the electrostatic regime ($\hat{\beta}=0.001$) for $\mathscr{C}=0.1$. In contrast, for $\mathscr{C}=5$ the effect of increasing $\hat{\beta}$ is to make the spectrum of E_k^M less steep. A different behavior of the spectral exponents of E_k for $\mathscr{C}=0.1$ and $\mathscr{C}=5$ was also observed. While the curve of E_k for $\hat{\beta}=10$ is steeper than the curve for $\hat{\beta}=0.001$ for $\mathscr{C}=0.1$, the opposite happens for $\mathscr{C}=5$. Therefore, the behavior of E_k is basically the same as E_k^N. When the value of $\hat{\beta}$ is increased the enstrophy spectra U_k are steeper for all values of $\mathscr{C}$. The effect of increasing $\hat{\beta}$ on the magnetic potential spectra A_k depends on the value of $\mathscr{C}$, but the spectral exponents do not have such strong changes as do the energy spectral exponents.

In Table III, the average values of k are shown for E, E^V, E^M, U, A, and P. In the case of the total energy E, for instance, the average k_m^E, is defined such that

$$(k_m^E)^2=\frac{\Sigma_k k^2 E_k}{\Sigma_k E_k}, \tag{39}$$

with analogous definitions for the other k_m. In the hydrodynamic regime ($\mathscr{C}=0.1$) and for $\mathscr{C}=1$, when $\hat{\beta}$ is increased the values of k_m^E, k_m^N (which is always the dominant component), k_m^U, k_m^A, and k_m^ϕ diminish, i.e., these fields have larger structures in the electromagnetic limit. It is important to notice that this effect is stronger in the case $\mathscr{C}=1$. In contrast, in the adiabatic limit $\mathscr{C}=5$, these fields have smaller structures for $\hat{\beta}=10$ than for $\hat{\beta}=0.001$, as in the latter the structures are already large. From the linear theory the value of $k_{\max}$ increases with β for all values of $\mathscr{C}$ (see also Fig. 1). For the runs in which a larger box was considered ($K_0=0.0375$) the spectra's maximum k_{SM} and the average wave numbers k_m, had approximately the same values.

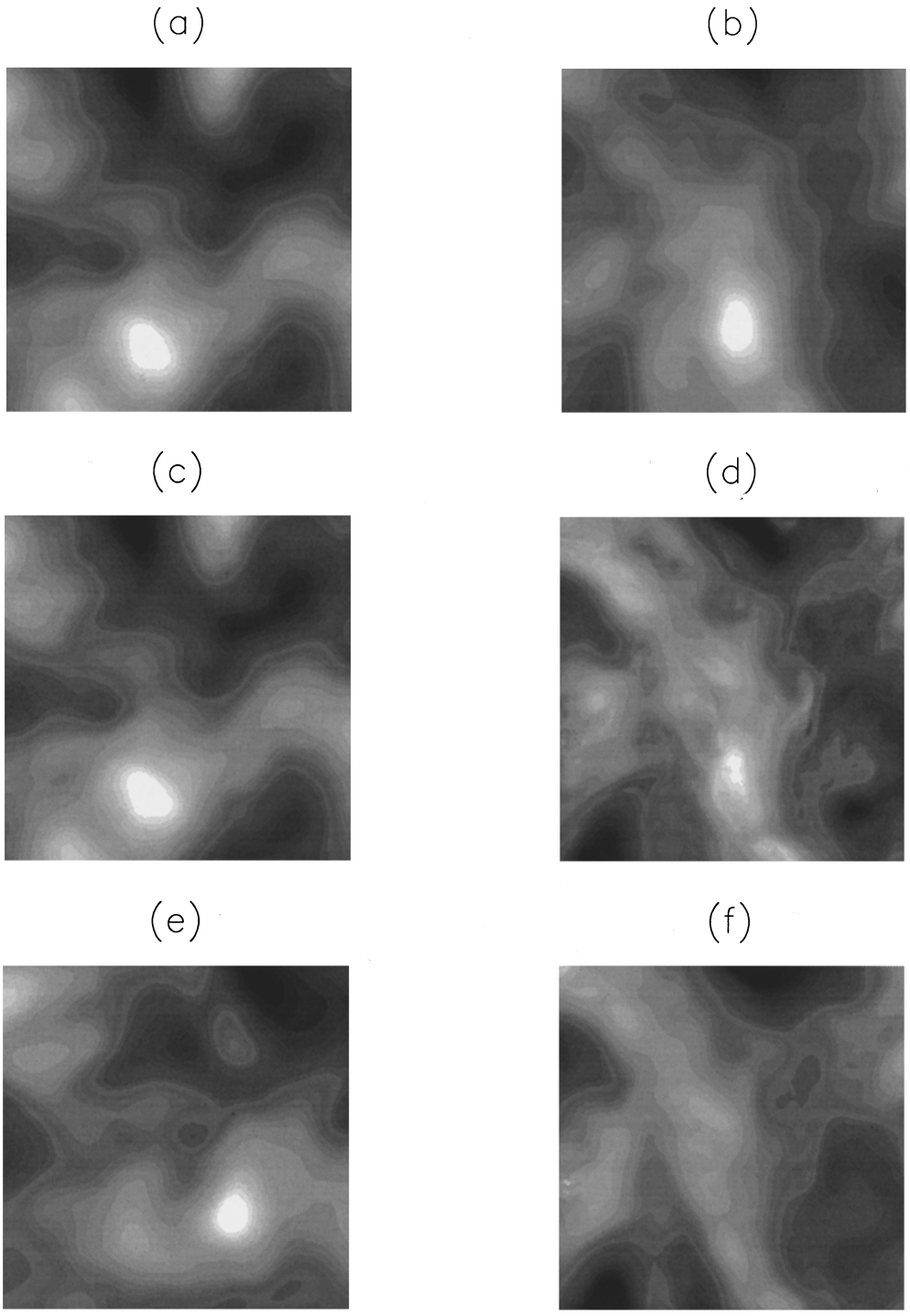

FIG. 4. Contour plots of $\tilde{\phi}$ [(a) and (b)], $\tilde{n}$ [(c) and (d)], and $\tilde{\psi}$ [(e) and (f)], for $\mathscr{C}=5$ in the electrostatic ($\hat{\beta}=0.001$) and electromagnetic ($\hat{\beta}=10$) regimes, respectively.

Therefore the structures did not become larger. All the other properties of the system remained the same, when a larger box was considered.

Another interesting feature comes from analyzing how the phase shifts between the main quantities are altered when $\hat{\beta}$ is increased and then comparing this with the linear phase shifts. In Fig. 7 we show the phase shifts obtained for $\mathscr{C}=5$ in the cases of $\hat{\beta}=0.001$ and $\hat{\beta}=10$. While in the electrostatic limit $\hat{\beta}=0.001$, δ_k^L and δ_k still had some resemblance for $\mathscr{C}=5$ [compare Figs. 2(a) and 7(a)], in the electromagnetic limit, this resemblance has completely disappeared. The same effect occurs for α_k^L and α_k with $\mathscr{C}=0.1$. The other linear and nonlinear phase shifts are very different in both the electrostatic and electromagnetic limits. Therefore, any small influence that the linear properties could still have on the turbulence in the electrostatic limit practically disappears for $\hat{\beta}=10$. This result is expected, as the linear growth rates are small in the electromagnetic limit—since magnetic in-

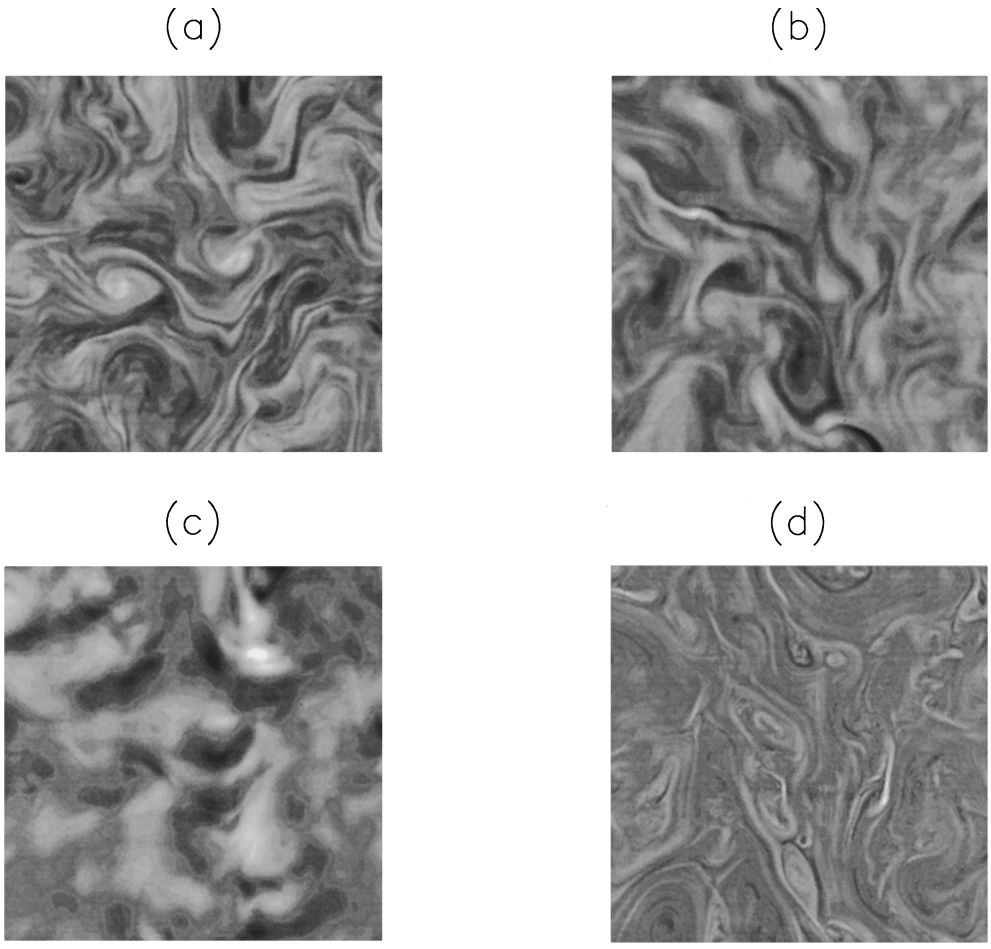

FIG. 5. Contour plots of $\tilde{\Omega}$ [(a) and (b)] and $\tilde{J}$ [(c) and (d)], for $\mathscr{C}=5$ in the electrostatic ($\hat{\beta}=0.001$) and electromagnetic ($\hat{\beta}=10$) regimes, respectively.

duction is reducing the coupling between $\tilde{n}$ and $\tilde{\phi}$, the linear effects are less able to compete with the nonlinear $E\times B$ advection for larger $\hat{\beta}$.

The transport flux, Γ_n, which is also the free energy source rate, is very much affected by the value of $\hat{\beta}$, diminishing as $\hat{\beta}$ increases (Table IV). This can be interpreted using the linear theory, which shows that the maximum of the linear growth rate $\gamma_{\max}$ diminishes for higher values $\hat{\beta}$ (Fig. 1) with a behavior similar to that of Γ_n, almost constant for $\hat{\beta}<1$, and quickly dropping for $\hat{\beta}>1$ (Fig. 8). The reason is the reduction of the coupling of $\tilde{n}$ to $\tilde{\phi}$ with increasing $\hat{\beta}$, making it more difficult for the free energy excited in $\tilde{n}$ by ∇n to return to $\tilde{\phi}$ and continue the driving.

V. LINEAR AND NONLINEAR SPECTRAL TRANSFER

The dynamical quantities which reveal the most information about the direction of cause and effect in a complicated turbulent system are the rates of transfer of invariants or pieces of invariants among different parts of the system.

TABLE II. Decay exponents for the invariants and energy components spectra in the different regimes. As might be expected from a strongly dissipative system, the spectra are not universal.

$\mathscr{C}$	$\hat{\beta}$	E_k	E_k^N	E_k^V	E_k^M	U_k	A_k
	0.001	$k^{-1.7}$	$k^{-1.6}$	$k^{-3.1}$	$k^{-3.4}$	$k^{-1.4}$	$k^{-5.4}$
0.1	0.1	$k^{-1.9}$	$k^{-1.8}$	$k^{-3.1}$	$k^{-3.4}$	$k^{-1.6}$	$k^{-5.5}$
	10	$k^{-3.2}$	$k^{-3.2}$	$k^{-3.5}$	$k^{-4.8}$	$k^{-2.1}$	$k^{-6.0}$
	0.001	$k^{-3.0}$	$k^{-2.8}$	$k^{-3.3}$	$k^{-4.4}$	$k^{-1.5}$	$k^{-6.6}$
1	0.1	$k^{-3.4}$	$k^{-3.0}$	$k^{-3.5}$	$k^{-4.8}$	$k^{-1.9}$	$k^{-6.5}$
	10	$k^{-4.5}$	$k^{-3.8}$	$k^{-5.0}$	$k^{-4.8}$	$k^{-2.1}$	$k^{-6.4}$
	0.001	$k^{-4.0}$	$k^{-4.6}$	$k^{-3.8}$	$k^{-6.0}$	$k^{-2.1}$	$k^{-7.5}$
5	0.1	$k^{-3.7}$	$k^{-4.2}$	$k^{-3.7}$	$k^{-5.8}$	$k^{-2.1}$	$k^{-7.7}$
	10	$k^{-3.2}$	$k^{-3.1}$	$k^{-3.9}$	$k^{-3.1}$	$k^{-2.5}$	$k^{-5.3}$

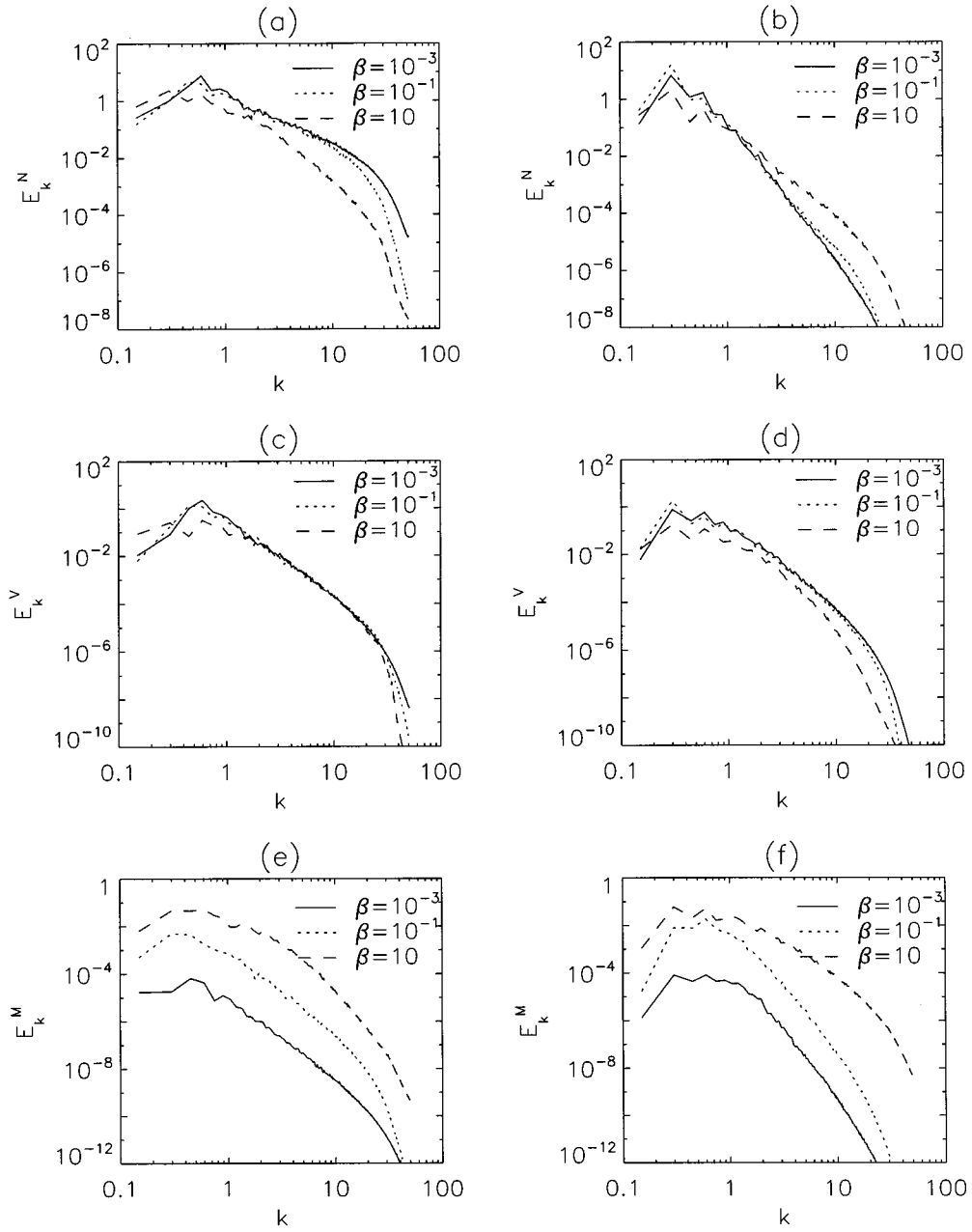

FIG. 6. Density spectra E_k^N for $\hat{\beta}=0.001,0.1,10$, $\mathscr{C}=0.1$ (a) and $\mathscr{C}=5$ (b). Kinetic energy spectra E_k^V for $\hat{\beta}=0.001,0.1,10$, $\mathscr{C}=0.1$ (c) and $\mathscr{C}=5$ (d). Magnetic energy spectra E_k^M for $\hat{\beta}=0.001,0.1,10$, $C=0.1$, (e), and $\mathscr{C}=5$ (f).

Linear transfer refers to exchanges between different dependent variables within each Fourier component or mode **k**, e.g., the transfer of fluctuation free energy between density and potential fluctuations mediated by the dissipative coupling through $\nabla_\parallel \tilde{J}$ in Eqs. (2) and (3) for $\tilde{n}$ and $\nabla_\perp^2\tilde{\phi}$. Nonlinear transfer, also called spectral transfer, refers to exchanges between different modes. This can occur within a given dependent variable, as, e.g., for **E×B** transferring density fluctuations free energy between two modes with different **k**. With magnetic fluctuations present, this mode–mode transfer can also occur between different dependent variables, as we shall see.

Such transfer analysis has proven very useful in understanding cascade phenomena in neutral fluid[52] and electrostatic drift-wave[36] turbulence. We now apply it to the electromagnetic drift-wave system.

A. Linear transfer

We now obtain the linear transfer of energy, enstrophy, and magnetic potential between the dependent variables $\tilde{\phi}$, $\tilde{n}$, and $\tilde{\psi}$ within a mode **k**. The linearized equations in Fourier space are

$$\frac{\partial\tilde{\Omega}(\mathbf{k})}{\partial t}=iK_\parallel\tilde{J}(\mathbf{k})-\mu k^4\tilde{\Omega}(\mathbf{k}), \tag{40}$$

TABLE III. Average wave numbers k_m for the invariants, the energy components, and P in the different regimes. Note especially the last two lines for $\mathscr{C}=1$ and 5: $\hat{\beta}$ affects enter most strongly in the most adiabatic regime.

$\mathscr{C}$	$\hat{\beta}$	k_m^E	k_m^N	k_m^V	k_m^M	k_m^U	k_m^A	k_m^ϕ
	0.001	1.35	1.43	0.90	0.76	1.58	0.42	0.56
0.1	0.1	1.34	1.41	0.90	0.75	1.57	0.42	0.55
	10	1.10	1.08	1.21	1.11	1.55	0.41	0.46
	0.001	1.12	1.05	1.21	1.02	1.59	0.69	0.82
1	0.1	1.09	1.02	1.19	0.99	1.55	0.67	0.81
	10	0.89	0.78	1.15	1.23	1.25	0.43	0.39
	0.001	0.53	0.49	0.65	0.67	0.64	0.50	0.48
5	0.1	0.45	0.40	0.69	0.80	0.63	0.53	0.37
	10	0.82	0.69	0.99	1.43	1.00	0.48	0.39

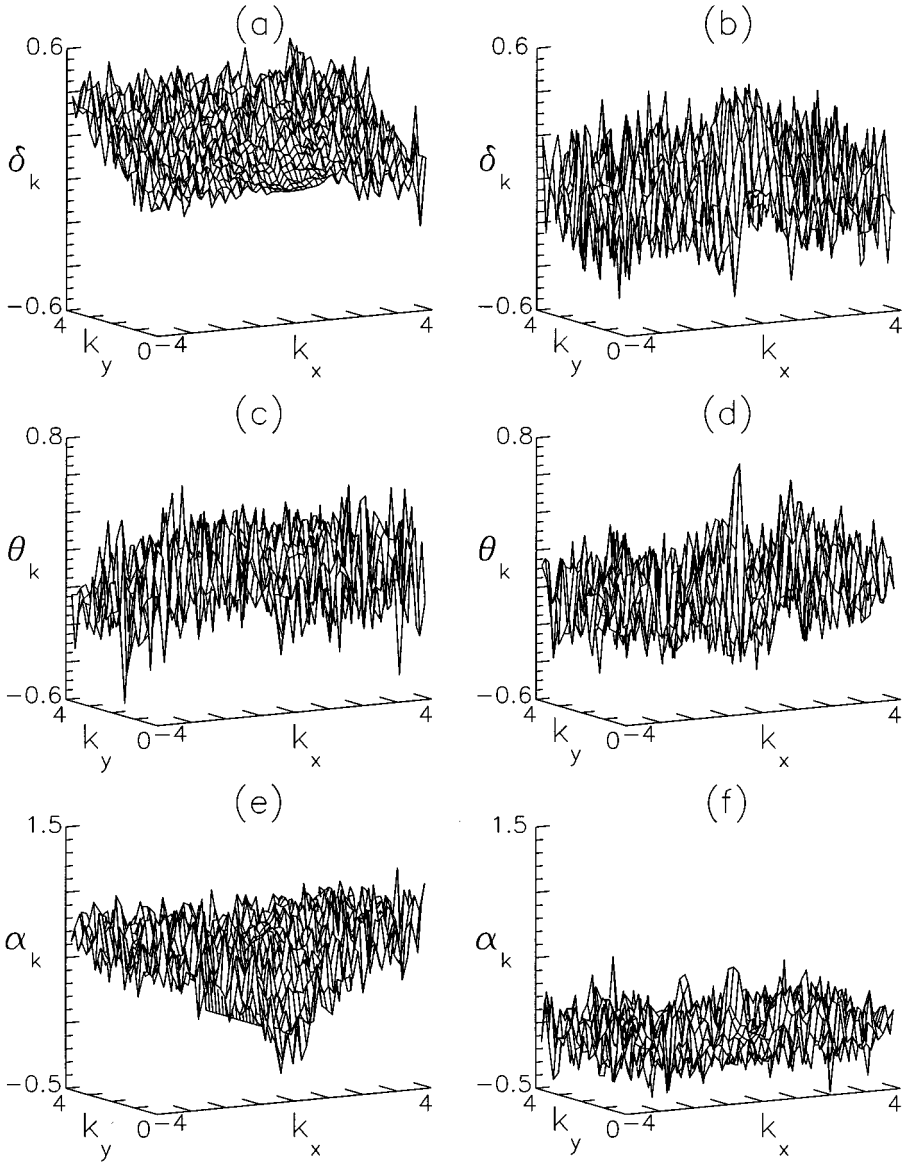

FIG. 7. Nonlinear phase shifts for $\mathscr{C}=5$. $\delta_{\mathbf{k}}$ for $\hat{\beta}=0.001$ (a) and $\hat{\beta}=10$ (b). $\theta_{\mathbf{k}}$ for $\hat{\beta}=0.001$ (c) and $\hat{\beta}=10$ (d). $\alpha_{\mathbf{k}}$ for $\hat{\beta}=0.001$ (e) and $\hat{\beta}=10$ (f).

TABLE IV. Total values of the source, transfer, and dissipation rates in the different regimes. High $\hat{\beta}$ has a strong quantitative effect for all three values of $\mathscr{C}$, but is most pronounced for the most adiabatic case, $\mathscr{C}=5$. Compare with the linear growth rates in Fig. 1.

$\mathscr{C}$	$\hat{\beta}$	Γ_n	Γ_p^N	Γ_p^V	Γ_r	Γ_a	Γ_d	$\mathscr{D}_N^E$	$\mathscr{D}_V^E$	$\mathscr{D}_M^E$	$\mathscr{D}^U$	$\mathscr{D}^A$
	0.001	3.4	1.9	-0.03	0.9	10^{-4}	-10^{-5}	1.2	0.03	10^{-7}	2.7	10^{-10}
0.1	0.1	3.3	1.9	-0.03	0.9	0.25	-0.008	1.1	0.03	10^{-5}	2.6	10^{-5}
	10	1.3	0.2	0.005	0.5	7.1	-0.004	0.2	0.04	0.007	1.1	0.07
	0.001	0.9	0.7	-0.03	0.3	10^{-4}	10^{-6}	0.04	0.03	10^{-6}	0.6	10^{-7}
1	0.1	0.9	0.9	-0.05	0.4	0.06	10^{-4}	0.04	0.04	10^{-4}	0.7	0.01
	10	0.2	0.02	-0.01	0.08	1.5	-0.002	0.03	0.01	0.01	0.2	0.3
	0.001	0.1	0.1	-0.01	0.07	-10^{-4}	-10^{-6}	0.003	0.01	10^{-6}	0.1	10^{-10}
5	0.1	0.1	0.1	-0.02	0.06	-0.02	10^{-4}	0.003	0.06	10^{-5}	0.1	10^{-5}
	10	0.09	0.01	-0.02	0.02	0.7	-0.002	0.02	0.006	0.02	0.08	0.09

$$\frac{\partial \tilde{n}(\mathbf{k})}{\partial t} = -ik_y \tilde{\phi}(\mathbf{k}) + iK_{\parallel}\tilde{J}(\mathbf{k}) - \mu k^4 \tilde{n}(\mathbf{k}), \tag{41}$$

$$\frac{\partial \tilde{\psi}(\mathbf{k})}{\partial t} = -ik_y \tilde{\psi}(\mathbf{k}) + iK_{\parallel}[\tilde{n}(\mathbf{k}) - \tilde{\phi}(\mathbf{k})] - D^{-1}\tilde{J}(\mathbf{k}) - \mu k^4 \tilde{\psi}(\mathbf{k}). \tag{42}$$

In Fourier space the invariants E, U, and A are given, respectively, by

$$E = \sum_{\mathbf{k}} E^V(\mathbf{k}) + E^N(\mathbf{k}) + E^M(\mathbf{k}) = \frac{1}{2}\sum_{\mathbf{k}} -\tilde{\Omega}(\mathbf{k})\tilde{\phi}(-\mathbf{k}) + \tilde{n}(\mathbf{k})\tilde{n}(-\mathbf{k}) + \tilde{J}(\mathbf{k})\tilde{\psi}(-\mathbf{k}), \tag{43}$$

$$U = \frac{1}{2}\sum_{\mathbf{k}} U(\mathbf{k}) = \frac{1}{2}\sum_{\mathbf{k}} [\tilde{n}(\mathbf{k}) - \tilde{\Omega}(\mathbf{k})][\tilde{n}(-\mathbf{k}) - \tilde{\Omega}(-\mathbf{k})], \tag{44}$$

$$A = \frac{1}{2}\sum_{\mathbf{k}} A(\mathbf{k}) = \frac{1}{2}\sum_{\mathbf{k}} \tilde{\psi}(\mathbf{k})\tilde{\psi}(-\mathbf{k}). \tag{45}$$

By using the definitions of each of the energy contributions given in Eqs. (43) and (40)–(42) we obtain the linear transfer of the energy components:

$$\frac{\partial E_L^V(\mathbf{k})}{\partial t} = -\Gamma_p^V(\mathbf{k}) - \mathscr{D}_V^E(\mathbf{k}), \tag{46}$$

$$\frac{\partial E_L^N(\mathbf{k})}{\partial t} = \Gamma_n(\mathbf{k}) - \Gamma_p^N(\mathbf{k}) - \mathscr{D}_N^E(\mathbf{k}), \tag{47}$$

$$\frac{\partial E_L^M(\mathbf{k})}{\partial t} = \Gamma_p^N(\mathbf{k}) + \Gamma_p^V(\mathbf{k}) - \Gamma_r(\mathbf{k}) - \mathscr{D}_M^E(\mathbf{k}). \tag{48}$$

The contribution of the electromagnetic transport fluxes (Γ_p^N and Γ_p^V) to the linear transfer of the total energy E is zero, although they have an important role in the linear energy transfer for each of the energy components.

The linear transfer for the enstrophy U and the magnetic potential A can be obtained in a similar way and are, respectively,

$$\frac{\partial U_L(\mathbf{k})}{\partial t} = \Gamma_n(\mathbf{k}) - \mathscr{D}^U(\mathbf{k}), \tag{49}$$

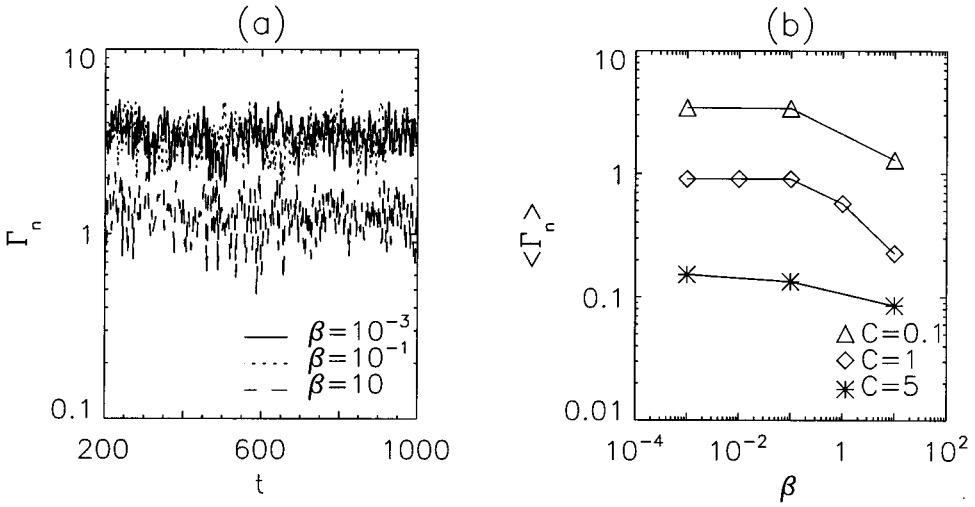

FIG. 8. Flux Γ_n for $\mathscr{C}=0.1$ and $\hat{\beta}=0.001,0.1,10$ (b). Variation of the average flux $\langle\Gamma_n\rangle$ with $\hat{\beta}$ for $\mathscr{C}=0.1$, $\mathscr{C}=1$, and $\mathscr{C}=5$.

$$\frac{\partial A_L(\mathbf{k})}{\partial t} = \Gamma_a(\mathbf{k}) - \Gamma_d(\mathbf{k}) - \mathscr{D}^A(\mathbf{k}). \tag{50}$$

The source, transfer, and dissipation rates in Fourier space are

$$\Gamma_p^V(\mathbf{k}) = -\frac{i}{2} K_\parallel [\tilde{\phi}(\mathbf{k})\tilde{J}(-\mathbf{k}) - \tilde{\phi}(-\mathbf{k})\tilde{J}(\mathbf{k})], \tag{51}$$

$$\Gamma_p^N(\mathbf{k}) = \frac{i}{2} K_\parallel [\tilde{n}(\mathbf{k})\tilde{J}(-\mathbf{k}) - \tilde{n}(-\mathbf{k})\tilde{J}(\mathbf{k})], \tag{52}$$

$$\Gamma_n(\mathbf{k}) = \frac{i}{2} k_y [\tilde{n}(\mathbf{k})\tilde{\phi}(-\mathbf{k}) - \tilde{n}(-\mathbf{k})\tilde{\phi}(\mathbf{k})], \tag{53}$$

$$\Gamma_r(\mathbf{k}) = D^{-1}\tilde{J}(\mathbf{k})\tilde{J}(-\mathbf{k}), \tag{54}$$

$$\Gamma_a(\mathbf{k}) = \frac{i}{2} K_\parallel \{[\tilde{\phi}(\mathbf{k}) - \tilde{n}(\mathbf{k})]\tilde{\psi}(-\mathbf{k}) - [\tilde{\phi}(-\mathbf{k}) - \tilde{n}(-\mathbf{k})]\tilde{\psi}(\mathbf{k})\}, \tag{55}$$

$$\Gamma_d(\mathbf{k}) = D^{-1}\tilde{\psi}(\mathbf{k})\tilde{J}(-\mathbf{k}), \tag{56}$$

$$\mathscr{D}^E(\mathbf{k}) = D_N^E(\mathbf{k}) + D_V^E(\mathbf{k}) + D_M^E(\mathbf{k}) = \mu k^4 [\tilde{n}(\mathbf{k})\tilde{n}(-\mathbf{k}) - \tilde{\Omega}(\mathbf{k})\tilde{\phi}(-\mathbf{k}) + \mathbf{k}^4\tilde{\psi}(\mathbf{k})\tilde{J}(-\mathbf{k})], \tag{57}$$

$$\mathscr{D}^U(\mathbf{k}) = \mu k^4 [\tilde{n}(\mathbf{k}) - \tilde{\Omega}(\mathbf{k})][\tilde{n}(-\mathbf{k}) - \tilde{\Omega}(-\mathbf{k})], \tag{58}$$

$$\mathscr{D}^A(\mathbf{k}) = \mu k^4 \tilde{\psi}(\mathbf{k})\tilde{\psi}(-\mathbf{k}). \tag{59}$$

In all of the formulas of this section, it is to be once again noted that since $K_\parallel = 1$, D is $\mathscr{C}$.

In Fig. 9 the linear transfer is shown for $\mathscr{C}=5$ in the electrostatic and electromagnetic regimes. The transfer rates are shown as a function of $k=|\mathbf{k}|$. In Table IV, the total values of the linear transfer are given in all regimes. In Fig. 10, the schematic direction of the linear and nonlinear transfer is shown. For $\mathscr{C}=0.1$ the linear transfer rates are approximately the same in the electrostatic and the electromagnetic regime. They look very similar to the case $\mathscr{C}=5$ and $\hat{\beta}=10$, apart from the sign of Γ_p^V.

Figure 9 and Table IV show that the dominant contribution of the linear transfer is given by Γ_n, which is the free energy source. The maximum of $\Gamma_n(k)$ is located at a $k\simeq 0.7$ for $\mathscr{C}=0.1$, which is very near the maximum of the energy spectrum E_k. By contrast, for $\mathscr{C}=5$ the maximum of $\Gamma_n(k)$ is located at $k\simeq 0.5$ and the maximum of E_k at $k\simeq 0.3$.

Another important contribution comes from $\Gamma_p^n(k)$, which is responsible for the linear transfer from $\tilde{n}$ to $\tilde{\psi}$. When $\hat{\beta}$ increases, $\Gamma_p^n(k)$ is located at smaller values of k. For $\mathscr{C}=15$ and $\hat{\beta}=0.001$, $\Gamma_p^n(k)$ has a negative contributionin the smaller values of k, which means that in this case the linear transfer is in the other direction—from $\tilde{\psi}$ to $\tilde{n}$ (Fig. 9). This effect disappears when $\hat{\beta}$ is increased. $\Gamma_p^V(k)$ is responsible for the linear transfer between $\tilde{\phi}$ and $\tilde{\psi}$. $\Gamma_p^V(k)$ is (in most cases) positive for the smaller values of k (linear transfer from $\tilde{\phi}$ to $\tilde{\psi}$) and negative for the higher values of k (linear transfer from $\tilde{\psi}$ to $\tilde{\phi}$), as can be seen in Fig. 9. The total contribution of $\Gamma_p^V(k)$ is (in most cases) negative, the main effect being therefore the transfer from $\tilde{\phi}$ to $\tilde{\psi}$ (see Table IV). It is interesting to note that in the electromagnetic limit, for $\mathscr{C}=0.1$, the total contribution of $\Gamma_p^V(k)$ is positive, while for $\mathscr{C}=5$, $\Gamma_p^V(k)$ is negative in the whole spectrum (Fig. 9). $\Gamma_r(k)$ (responsible for the resistive dissipation) has a more important role for $\mathscr{C}=0.1$ than for $\mathscr{C}=5$. By increasing $\hat{\beta}$, Γ_r is dislocated for higher values of k. $\Gamma_a(k)$, which is the source of the magnetic potential, has a strong dependence with $\hat{\beta}$, with its values increasing dramatically with increasing β and its maximum being dislocated to much smaller values of k.

B. Nonlinear spectral transfer

We now compute the nonlinear spectral transfer of the different invariants between different **k** modes, both within and between the dependent variables. By considering only the nonlinear terms of the equations, we obtain for the nonlinear energy transfer:

$$\frac{\partial E^V(\mathbf{k})}{\partial t} = \sum_{\mathbf{q}} [T^V(\mathbf{k}\leftarrow\mathbf{q}) + T_1^{VM}(\mathbf{k}\leftarrow\mathbf{q})], \tag{60}$$

$$\frac{\partial E^N(\mathbf{k})}{\partial t} = \sum_{\mathbf{q}} [T^N(\mathbf{k}\leftarrow\mathbf{q}) + T_1^{NM}(\mathbf{k}\leftarrow\mathbf{q})], \tag{61}$$

$$\frac{\partial E^M(\mathbf{k})}{\partial t} = \sum_{\mathbf{q}} [T_2^{VM}(\mathbf{k}\leftarrow\mathbf{q}) + T_2^{NM}(\mathbf{k}\leftarrow\mathbf{q})], \tag{62}$$

where the spectral transfer rates of energy from mode **q** to mode **k** are given by

$$T^V(\mathbf{k}\leftarrow\mathbf{q}) = 2(k_x q_y - q_x k_y)\mathrm{Re}[\tilde{\phi}(-\mathbf{k})\tilde{\Omega}(\mathbf{k}-\mathbf{q})\tilde{\phi}(\mathbf{q})], \tag{63}$$

$$T_1^{VM}(\mathbf{k}\leftarrow\mathbf{q}) = -2\frac{1}{\hat{\beta}}(k_x q_y - q_x k_y)\mathrm{Re}[\tilde{\phi}(-\mathbf{k}) \times \tilde{\psi}(\mathbf{k}-\mathbf{q})\tilde{J}(\mathbf{q})], \tag{64}$$

$$T_2^{VM}(\mathbf{k}\leftarrow\mathbf{q}) = -2\frac{1}{\hat{\beta}}(k_x q_y - q_x k_y)\mathrm{Re}[\tilde{J}(-\mathbf{k}) \times \tilde{\psi}(\mathbf{k}-\mathbf{q})\tilde{\phi}(\mathbf{q})], \tag{65}$$

$$T^N(\mathbf{k}\leftarrow\mathbf{q}) = 2(k_x q_y - q_x k_y)\mathrm{Re}[\tilde{n}(-\mathbf{k})\tilde{\phi}(\mathbf{k}-\mathbf{q})\tilde{n}(\mathbf{q})], \tag{66}$$

$$T_1^{NM}(\mathbf{k}\leftarrow\mathbf{q}) = 2\frac{1}{\hat{\beta}}(k_x q_y - q_x k_y)\mathrm{Re}[\tilde{n}(-\mathbf{k}) \times \tilde{\psi}(\mathbf{k}-\mathbf{q})\tilde{J}(\mathbf{q})], \tag{67}$$

$$T_2^{NM}(\mathbf{k}\leftarrow\mathbf{q}) = 2\frac{1}{\hat{\beta}}(k_x q_y - q_x k_y)\mathrm{Re}[\tilde{J}(-\mathbf{k}) \times \tilde{\psi}(\mathbf{k}-\mathbf{q})\tilde{n}(\mathbf{q})]. \tag{68}$$

It is important to understand how this transfer occurs. By considering now the mode **q**, we have

$$\frac{\partial E_V(\mathbf{q})}{\partial t} = -\sum_{\mathbf{q}} [T_V(\mathbf{k}\leftarrow\mathbf{q}) + T_2^{VM}(\mathbf{k}\leftarrow\mathbf{q})], \tag{69}$$

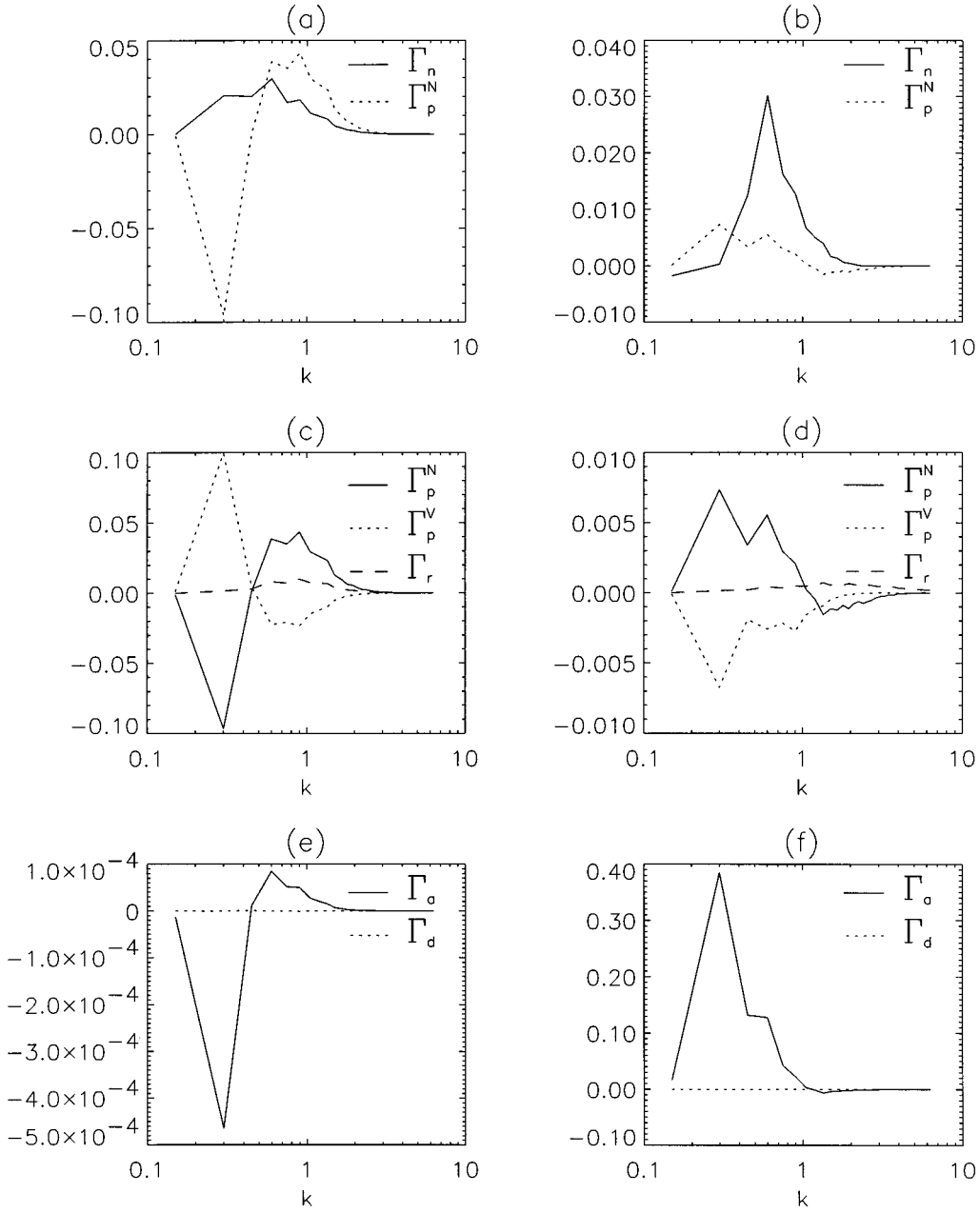

FIG. 9. Linear transfer rates for $\mathscr{C}=5$, with $\hat{\beta}=0.001$ [(a), (c), and (e)] and $\hat{\beta}=10$ [(b), (d), and (f)].

$$\frac{\partial E^N(\mathbf{q})}{\partial t} = -\sum_{\mathbf{q}} \left[T^N(\mathbf{k}\leftarrow\mathbf{q}) + T_2^{NM}(\mathbf{k}\leftarrow\mathbf{q}) \right], \tag{70}$$

$$\frac{\partial E^M(\mathbf{q})}{\partial t} = -\sum_{\mathbf{q}} \left[T_1^{VM}(\mathbf{k}\leftarrow\mathbf{q}) + T_1^{NM}(\mathbf{k}\leftarrow\mathbf{q}) \right]. \tag{71}$$

Therefore, the purely kinetic and density transfer rates are transferred in a direct way (between different modes of the same fluctuation field), while the mixed magnetic–kinetic and magnetic-density transfer rates represent nonlinear transfer between modes of $\tilde{n}$ and $\tilde{\psi}$ or $\tilde{\phi}$ and $\tilde{\psi}$. That is, the $\mathbf{E}\times\mathbf{B}$ transfer remains within a given dependent variable, but the magnetic transfer occurs between different dependent variables. Each of the mixed nonlinear transfer rates (T_1^{VM}, T_2^{VM}, T_1^{NM}, and T_2^{NM}) is not symmetric by itself, a sum must be defined in order to obtain transfer rates with a definition equivalent to the other transfer rates. T^{VM} and T^{NM} are defined, respectively, as $T^{VM}(\mathbf{k}\leftarrow\mathbf{q})=T_1^{VM}(\mathbf{k}\leftarrow\mathbf{q})+T_2^{VM}(\mathbf{k}\leftarrow\mathbf{q})$ and $T^{NM}(\mathbf{k}\leftarrow\mathbf{q})=T_1^{NM}(\mathbf{k}\leftarrow\mathbf{q})+T_2^{NM}(\mathbf{k}\leftarrow\mathbf{q})$. The resulting effect of the mixed transfer rates is then given by T^{VM} and T^{NM}, which then define the character of the nonlinear transfer. A schematic form of the nonlinear and the linear transfer of energy can be found in Fig. 10.

We are also interested in the spectral transfer of the en-

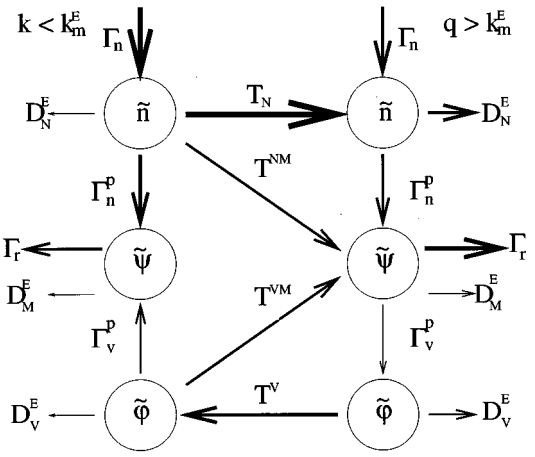

FIG. 10. Nonlinear and linear energy transfer processes among the variables $\tilde{n}$, $\tilde{\phi}$, and $\tilde{\psi}$ for $\mathscr{C}=0.1$ and $\hat{\beta}=10$.

strophy U and the magnetic potential A, as defined in Eqs. (44) and (45), respectively. We obtain:

$$\frac{\partial U(\mathbf{k})}{\partial t}=\sum_{\mathbf{q}} T^U(\mathbf{k}\leftarrow\mathbf{q})=\sum_{\mathbf{q}} 2(k_x q_y-q_x k_y)\mathrm{Re}[\tilde{n}(-\mathbf{k}) -\tilde{\Omega}(-\mathbf{k})]\tilde{\phi}(\mathbf{k}-\mathbf{q})[\tilde{n}(\mathbf{q})-\tilde{\Omega}(\mathbf{q})], \tag{72}$$

$$\frac{\partial A(\mathbf{k})}{\partial t}=\sum_{\mathbf{q}} T^A(\mathbf{k}\leftarrow\mathbf{q})=\sum_{\mathbf{q}} 2(k_x q_y-q_x k_y)\mathrm{Re}\ \tilde{\psi}(-\mathbf{k}) \times[\tilde{\phi}(\mathbf{k}-\mathbf{q})-\tilde{n}(\mathbf{k}-\mathbf{q})]\tilde{\psi}(\mathbf{q}). \tag{73}$$

In Fig. 11 the nonlinear transfer of the energy components are shown for $C=5$ for the electrostatic and the electromagnetic regimes. In Fig. 12 the nonlinear transfer of the three invariants of the system (E, U, and A) is shown in the electrostatic and the electromagnetic regimes for $\mathscr{C}=5$. In Figs. 11 and 12, contours of $T(\mathbf{k}\leftarrow\mathbf{q})$ are shown only where

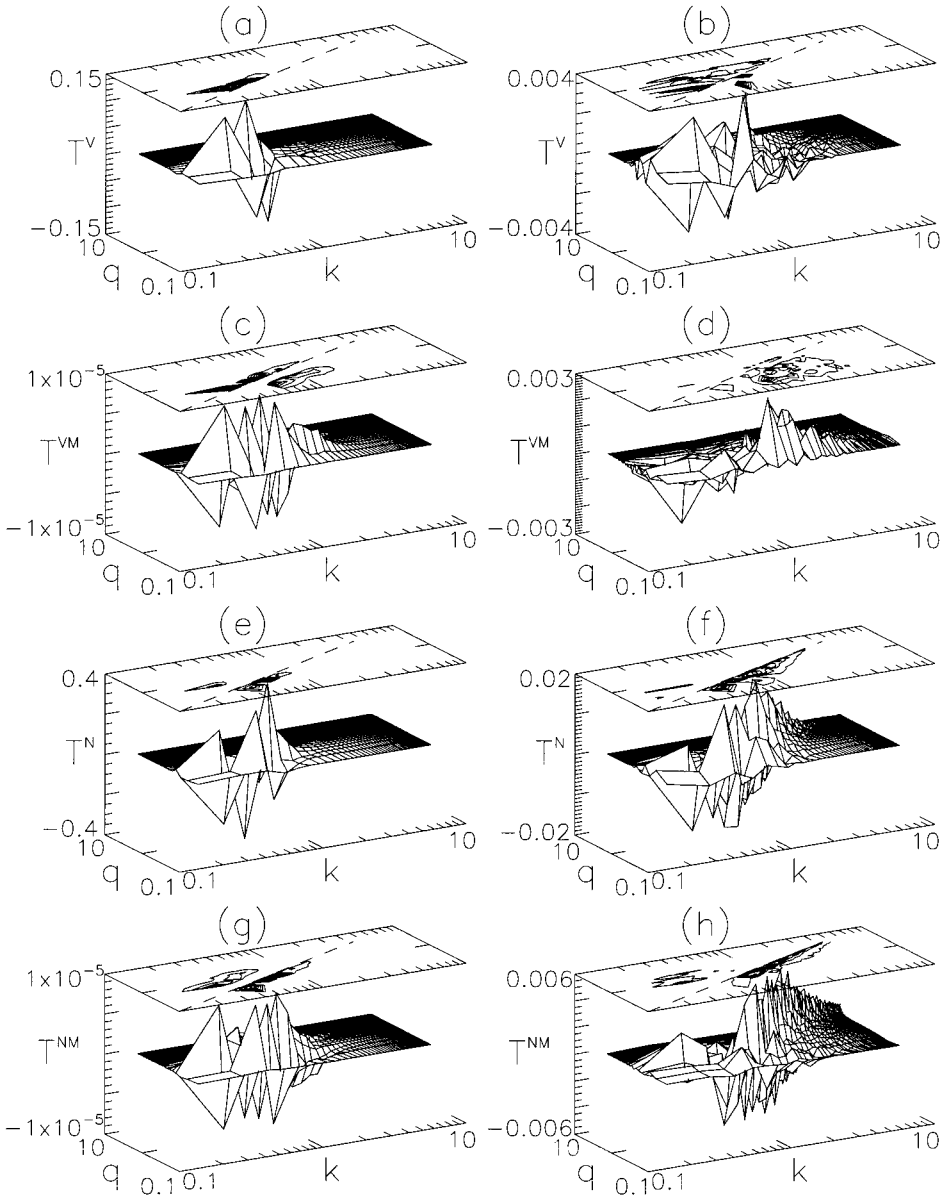

FIG. 11. Nonlinear transfer rates of the energy components for $\mathscr{C}=5$, $\hat{\beta}=0.001$ [(a), (c), (e), and (g)] and $\hat{\beta}=10$ [(b), (d), (f), and (b)].

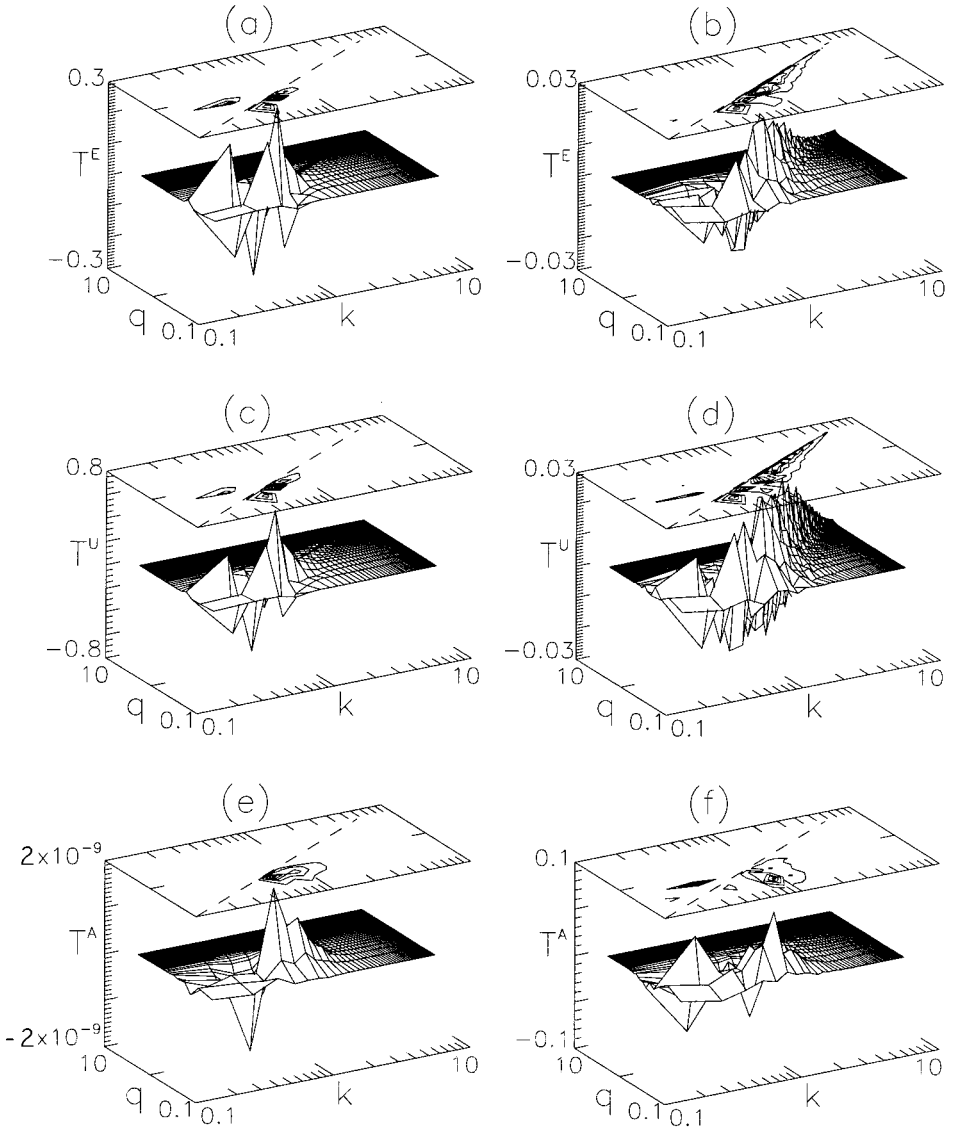

FIG. 12. Nonlinear transfer rates of the invariants for $\mathscr{E}=5$, $\hat{\beta}=0.001$ [(a), (c), and (e)] and $\hat{\beta}=10$ [(b), (d), and (f)].

it is positive, since by definition the nonlinear transfer functions are antisymmetric about the line $k=q$ (dashed line drawn in Figs. 11 and 12), which corresponds to the exchange $(k\leftrightarrow q)$. Further clarifying the behavior of $T(\mathbf{k}\leftarrow\mathbf{q})$ is the surface of T as a function of k and q. The variation of the maximum values of the nonlinear transfer in the different regimes is given in Table V. From Figs. 11 and 12, one can see that most of the activity of the nonlinear transfer func-

TABLE V. Maximum values of the nonlinear transfer rates in the different regimes. Note that the contributions to the electromagnetic nonlinear transfer (T^{NM} and T^{VM}, tracking the electromagnetic corrections to $\boldsymbol{\nabla}_\parallel$) are always small compared to their linear counterparts in Table IV (Γ_p^N and Γ_p^V, tracking the linear, unperturbed $\boldsymbol{\nabla}_\parallel$). This indicates that the electromagnetic contributions to transport are likewise small.

$\mathscr{E}$	$\hat{\beta}$	$T^N_{\max}$	$T^V_{\max}$	$T^{NM}_{\max}$	$T^{VM}_{\max}$	$T^E_{\max}$	$T^U_{\max}$	$T^A_{\max}$
	0.001	1.29	0.23	10^{-6}	10^{-6}	1.16	2.03	10^{-8}
0.1	0.1	1.45	0.30	0.001	10^{-4}	1.15	2.24	10^{-4}
	10	0.24	0.02	0.01	0.006	0.23	0.33	0.19
	0.001	0.12	0.08	10^{-5}	10^{-5}	0.06	0.33	10^{-8}
1	0.1	0.19	0.13	0.001	0.001	0.07	0.39	10^{-4}
	10	0.03	0.004	0.007	0.003	0.03	0.05	0.10
	0.001	0.38	0.11	10^{-5}	10^{-5}	0.27	0.60	10^{-9}
5	0.1	0.22	0.09	0.001	0.001	0.17	0.31	10^{-4}
	10	0.02	0.003	0.005	0.002	0.02	0.02	0.06

TABLE VI. Cascade type of the nonlinear transfer processes in the different regimes. Only the $E\times B$ inverse cascade (T^V) is affected by the magnetic fluctuations, and only at high $\hat{\beta}$.

$\mathscr{C}$	$\hat{\beta}$	T^N	T^V	T^{NM}	T^{VM}	T^E	T^U	T^A
	0.001	direct	inverse	mixed	direct	direct	direct	direct
0.1	0.1	direct	inverse	mixed	mixed	direct	direct	direct
	10	direct	inverse	direct	direct	direct	direct	direct
	0.001	direct	inverse	mixed	mixed	direct	direct	mixed
1	0.1	direct	inverse	mixed	mixed	direct	direct	direct
	10	direct	mixed	direct	direct	direct	direct	direct
	0.001	direct	inverse	mixed	mixed	mixed	mixed	direct
5	0.1	direct	inverse	mixed	mixed	direct	direct	direct
	10	direct	mixed	direct	direct	direct	direct	mixed

tions is close to the line $k=q$, which shows that the transfer occurs between scales of motion of similar scale, the transfer may be then properly described as a local cascade. When the positive contours lie above the $k=q$ line, there is an inverse cascade, toward large scales. A direct cascade, toward small scales, is specified when the positive contours are under the $k=q$ line. When the positive contours appear simultaneously above and under the $k=q$ line, without a clear dominant behavior, a mixed cascade is defined, with the transfer occurring simultaneously to both large and small scales. The cascade type for each of the nonlinear transfer contributions is given in Table VI.

In all cases, the dominant nonlinear transfer is T^N, as seen in Fig. 11 and Tables V and VI. Even in the electromagnetic regime, the terms responsible for the magnetic transfer of the energy, T^{NM} and T^{VM}, are much smaller than T^N. T^N shows a direct cascade, as $\tilde{n}$ is passively advected by the **E×B** flow eddies. Even in the case $\mathscr{C}=5$, which is the most sensitive to changes of $\hat{\beta}$, T^N always has the same character, showing a direct cascade, with only the magnitude of T^N being sensitive to variations of $\hat{\beta}$a nd $\mathscr{C}$. T^V shows an inverse cascade in the electrostatic limit. However, this character is modified when $\hat{\beta}$ is increased for $\mathscr{C}=1$ and $\mathscr{C}=5$ (mixed cascade), while the inverse cascade remain robust for $\mathscr{C}=0.1$. The direct cascade contribution of T^V is already present in the electrostatic limit. Nevertheless, as the inverse cascade contribution is very strong, the direct cascade contribution cannot be seen in the contour plots. As $\hat{\beta}$ increases, the inverse contribution of T^V becomes weaker. Therefore, in the electromagnetic limit the direct contribution of T^V becomes more important and a mixed cascade appears (for $\mathscr{C}=1$ and $\mathscr{C}=5$). It is interesting to note that the dual cascade, which was observed for the Hasegawa–Wakatani system,[36] with an inverse cascade of the electric potential and a direct cascade of the vorticity is still present in the electrostatic case. For increasing $\hat{\beta}$, the vorticity continues to show a direct cascade. However, the electric potential sometimes presents a mixed cascade instead of the inverse cascade.

The nonlinear transfer rates involving the magnetic fluctuations $\tilde{\psi}$, T^{NM}, and T^{VM}, are very small (negligible) in the electrostatic limit, as expected. In this limit, T^{NM} and T^{VM} have a mixed cascade character. As $\hat{\beta}$ increases, the direct cascade becomes stronger until in the electromagnetic limit, the direct cascade is clearly dominant for all values of $\mathscr{C}$. By comparing the electrostatic limit with the electromagnetic limit, we can conclude that the magnetic fluctuations make the transfer of energy between the density and the potential fluctuations more difficult. Therefore the response of the potential fluctuations $\tilde{\phi}$ to the density fluctuations $\tilde{n}$ is delayed, leading to the loss of adiabaticity in the electromagnetic limit. That this is principally a linear effect may be seen from the weakness of the nonlinear magnetic transfer rates, which are always very small compared to their linear counterparts, Γ_p^N and Γ_p^V. The appropriate conclusion is that the only really significant electromagnetic effect in this system is magnetic induction. Nevertheless, its action to enhance the nonadiabatic character of the overall system remains important in the turbulent regime.

The resulting nonlinear energy transfer, T^E, is strongly dominated by T^N in all cases considered. For $\mathscr{C}=0.1$, T^E shows a direct cascade independent of $\hat{\beta}$ (see Table VI). In the adiabatic regime ($\mathscr{C}=5$) for $\hat{\beta}=0.001$, T^E has a mixed cascade character, since in this limit T^V has an important role. As $\hat{\beta}$ increases this role diminishes and T^E shows the usual direct cascade (see also Fig. 12 and Table V). The nonlinear transfer of the enstrophy T^U shows a direct cascade, except in the case $\mathscr{C}=5$ and $\hat{\beta}=0.001$. In this case the kinetic transfer has a more important role, changing the character of the transfer to a mixed cascade. However, even in this case the dominant behavior is the direct cascade. Therefore, the main effect of $\hat{\beta}$ on T^U is to change its magnitude, with the qualitative behavior of the nonlinear transfer being rather robust. T^A is the quantity that is most affected by $\hat{\beta}$. Besides the expected increase of the magnitude of T^A, its qualitative behavior depends strongly on β and $\mathscr{C}$ (Fig. 12). For $\mathscr{C}=0.1$ and $\hat{\beta}=0.001$, T^A presents a direct local cascade. When $\hat{\beta}=10$ the cascade is still direct, but involves a rather different range of modes, not so near the line $k=q$ (local cascade). On the other hand, for $\mathscr{C}=5$, while the electrostatic limit is very similar to that of $\mathscr{C}=0.1$, the electromagnetic limit has a mixed local cascade character.

In Fig. 10 we summarize in schematic form the linear and nonlinear transfer of energy of the system. This diagram is more complicated than the ones obtained for electrostatic models,[49,50] but its meaning is the same. We chose as a typical example the case $\mathscr{C}=0.1$ and $\hat{\beta}=10$. Each of the circles represents a batch of wave numbers in one of the three de-

pendent variables at lower and higher k, on the left- and right-hand sides, respectively. The boundary between low and high k is chosen as k_m^E. Each of the arrows between two of the circles represents a transfer rate as computed from the results according to the definitions in this section. Each of the arrows pointing into or out of a circle from boundary represents one of the source or sink rates, respectively, as computed from the results according to the definitions in Sec. II B. The thickness of each arrow is logarithmically proportional to the computed strength of the rate it represents. Although the direction of each nonlinear transfer process is given by its arrow, it is important to note that the sum of all the nonlinear transfer rates is zero, by definition. The sum of the linear transfer rates is also zero, but this is only due to the fact that the turbulence is well saturated.

The source of fluctuation free energy Γ_n is present at both low and high k, but is stronger at low k. The energy is then linearly transferred from $\tilde{n}$ to $\tilde{\psi}$ through Γ_n^p, while being dissipated in the smaller scales by D_N^E, D_M^E, and Γ_r. Simultaneously the energy is being transferred nonlinearly from $\tilde{n}$ at low k to $\tilde{n}$ at high k in a direct cascade, represented by T^N. The energy in $\tilde{n}$ at low k is also transferred to $\tilde{\psi}$ at high k, also a direct cascade. Figure 10 shows clearly how the presence of $\tilde{\psi}$ makes it difficult to transfer energy directly from $\tilde{n}$ to $\tilde{\phi}$, which is how it goes in an electrostatic model.[36,49] At high k there is a weak linear transfer from $\tilde{\psi}$ to $\tilde{\phi}$ through Γ_V^p, but at low k, Γ_V^p is in the opposite direction. The energy in $\tilde{\phi}$ at low k is also sent to $\tilde{\psi}$ at high k through T^{VM} in a direct cascade. Finally there is the strong nonlinear inverse cascade between high- and low-k $E\times B$ energy in $\tilde{\phi}$. Most of the hyperviscous dissipation is in $\tilde{\phi}$ at high k, reflecting the power of the $E\times B$ vorticity cascade. The strongest dissipation process is resistivity, however, reflected by Γ_r.

An important result of this energy transfer study has been to determine that not only the total particle transport is zero,[26] but each contribution to the nonlinear electromagnetic dynamics is itself small compared to the free energy excitation rate represented by Γ_n. This tells us that the part of the system's dynamics which determines the turbulent transport is still largely electrostatic, even if the magnetic induction has changed its overall level. Figure 10 shows clearly however that the role of the magnetic fluctuations in the system is still important to the energy transfer, even though the nonlinear transfer rates involving the magnetic fluctuations are comparatively small. The magnetic fluctuations interfere with the coupling between the density and potential fluctuations, reducing its immediacy. It is important to note that the energy transfer character is in agreement with the electrostatic studies.[36,49] The magnetic fluctuations do not change the character of the nonlinear transfer T^N and T^V in the electrostatic system at all, but they do change the linear transfer, which instead of going directly between $\tilde{n}$ and $\tilde{\phi}$ must go through $\tilde{\psi}$.

VI. CONCLUSION

In this paper, we have presented detailed properties of the turbulent states of a simple drift-wave model with magnetic fluctuations. The system was solved numerically and compared with the known properties of its limiting cases, the 2-D Hasegawa–Wakatani and MHD equations.

The most important single conclusion is that although in certain limits the magnetic fluctuations have significant influence (near-adiabatic electrons, high $\hat{\beta}$), the turbulence is largely electrostatic in character. This is particularly true with regard to the transport, as shown by the energy transfer study in Sec. V. For the saturated amplitude and mode structure, we observed dominant magnetic influence only when $\hat{\beta}$ was as large as 10, in contrast to nominal scaling which usually puts the boundary at $\hat{\beta}\sim 1$. And even then, the actual transport was still dominantly electrostatic even in basic character. The magnetic part of the system was seen to be effective in enhancing the nonadiabatic character of the electron dynamics. In turbulence in a sheared magnetic field, the electron nonadiabaticity is already strongly enhanced, so that a preliminary study saw little effect of the magnetic fluctuations in the collisional regime.[46] However, the present results suggest that the hot plasma regime ($T>1$ keV) may be made less adiabatic than would be otherwise expected. Work is underway on a three-dimensional model which will test this directly in tokamak geometry.

In any case, the neglect of magnetic fluctuations should be done with extreme care, since as was seen in the energy transfer analysis, the magnetic part of the system has an important influence on the relation between density and electrostatic fluctuations, i.e., the nonadiabatic dynamics which determines the transport. Therefore, even if the turbulence can still be considered electrostatic, it is of importance to understand the role of the magnetic fluctuations in determining the characteristics of the turbulence in more realistic models.

[1] P. Liewer, Nucl. Fusion **25**, 543 (1985).
[2] A. J. Wootton, B. A. Carreras, H. Matsumoto, K. McGuire, W. A. Peebles, Ch. P. Ritz, P. W. Terry, and S. J. Zweben, Phys. Fluids B **2**, 2879 (1990).
[3] W. Horton, Phys. Rep. **192**, 1 (1990).
[4] J. W. Connor, Plasma Phys. Controlled Fusion **35**, B293 (1993).
[5] K. H. Burrell, K. W. Gentle, N. C. Luthman, Jr., E. S. Marmar, M. Murakami, K. F. Schoenberg, W. M. Tang, and M. C. Zarnstorff, Phys. Fluids B **2**, 2905 (1990).
[6] A. H. Boozer, D. E. Baldwin, C. W. Horton, R. R. Dominguez, A. H. Glasser, J. A. Krommes, G. H. Neilson, K.-C. Shaing, W. L. Sadowski, and H. Weitzner, Phys. Fluids B **2**, 2870 (1990).
[7] H. Ji, H. Toyama, K. Miyamoto, S. Shinohara, and A. Fujisawa, Phys. Rev. Lett. **67**, 62 (1991).
[8] G. Fiksel, S. C. Prager, W. Shen, and M. Stoneking, Phys. Rev. Lett. **72**, 1028 (1994).
[9] G. X. Li, A. Möller, J. R. Drake, H. Bergsåker, J. H. Brzozowski, G. Hellblom, S. Mazur, P. Nordlund, and A. Welander, in *Europhysics Conference Abstracts, Proceedings of the 22nd European Physical Society Conference on Controlled Fusion and Plasma Physics*, Bournemouth, 1995, edited by B. E. Keen, P. E. Stott, and J. Winter (European Physical Society, Petit-Lancy, 1995), Vol. 19C, p. I-173.
[10] TEXT: Texas Experimental Tokamak was in operation at the Fusion Research Center, University of Texas at Austin until ~1990. See K. W. Gentle, Nucl. Technol./Fusion **1**, 479 (1981).
[11] A. J. Wootton, R. Bengtson, R. V. Bravenec, J. Chen G. Cima, P. H. Edmonds, M. Freeman, H. Gasquet, K. Gentle, G. Hallock, Y. Karzhavin, S. McCool, D. Patterson, P. Phillips, B. Richards, D. Roberts, W. Rowan, D. Ross, E. Solano, D. Sing, R. F. Steimle, H. Tsui, J. Uglum, Y. Wen, Z. Zhang, R. F. Gandy, T. D. Rempel, M. Kwon, C. Watts, R. Durst, R. J. Fonck, D. L. Brower, Y. Jiang, W. A. Peebles, J. W. Heard, R. L. Hickock, A. Ouroua, P. M. Schoch, K. A. Connor, and G. Giruzzi, ''The role of fluctuations in determining transport in TEXT,'' to be published in *Plasma Physics and Controlled Nuclear Fusion Research, Proceedings of*

the 15th International Conference, Seville, 1994 (International Atomic Energy Agency, Vienna, 1995).
[12]C. Hidalgo, Plasma Phys. Controlled Fusion **37**, A53 (1995).
[13]J. W. Connor and H. R. Wilson, Plasma Phys. Controlled Fusion **36**, 719 (1994).
[14]X. Garbet, F. Mourgues, and A. Samain, Plasma Phys. Controlled Fusion **32**, 917 (1990).
[15]A. Hirose, A. I. Smolyakov, M. Elia, L. Zhang, and O. Ishihara, Comm. Plasma Phys. Controlled Fusion **16**, 141 (1995).
[16]B. B. Kadomtsev and O. P. Potguse, in *Plasma Physics and Controlled Nuclear Fusion Research, Proceedings of the 7th International Conference*, Innsbruck, 1978 (International Atomic Energy Agency, Vienna, 1979), Vol. 1, p. 649.
[17]F. A. Haas, A. Thyagaraja, and I. Cook, Plasma Phys. **23**, 1027 (1981).
[18]B. A. Carreras, P. H. Diamond, M. Murakami, J. L. Dunlap, J. D. Bell, H. R. Ricks, J. A. Holmes, E. A. Lazarus, V. K. Pare, P. Similon, C. E. Thomas, and R. M. Wieland, Phys. Rev. Lett. **50**, 503 (1983).
[19]M. A. Dubois, P. Ghendrih, B. Pégourié, R. Sabot, A. Samain, M. Zabiégo, and X. L. Zou, Plasma Phys. Controlled Fusion **36**, B55 (1994).
[20]D. Biskamp, *Nonlinear Magnetohydrodynamics* (Cambridge University Press, Cambridge, 1993).
[21]D. Montgomery, in *Lecture Notes on Turbulence*, edited by J. R. Herring and J. C. McWilliams (World Scientific, Singapore, 1988), p. 75.
[22]J. D. Callen, Phys. Rev. Lett. **39**, 1540 (1977).
[23]P. A. Duperrex, Ch. Hollenstein, B. Joye, R. Keller, J. B. Lister, F. B. Marcus, J. M. Moret, A. Pochelon, and W. Simm, Phys. Lett. A **106**, 133 (1984).
[24]TCA: The first of a series of tokamak experiments at Lausanne, Switzerland, having entered operation in 1980. See A. D. Cheetham, A. Heym, F. Hofmann, K. Hruska, R. Keller, A. Leitti, J. B. Lister, A. Pochelon, H. Ripper, A. Simik, and A. Teuszel, *Proceedings, 11th SOFT* (Oxford University Press, London, 1980), Vol. 1, p. 601.
[25]K. Molvig, S. P. Hirshman, and J. C. Whitson, Phys. Rev. Lett. **43**, 582 (1979).
[26]R. E. Waltz, Phys. Fluids **28**, 577 (1985).
[27]E. Fernandez, P. W. Terry, and D. E. Newman, Phys. Plasmas **2**, 4204 (1995).
[28]A. A. Thoul, P. L. Similon, and R. N. Sudan, Phys. Plasmas **1**, 601 (1994).
[29]P. W. Terry, P. H. Diamond, and T. S. Hahm, Phys. Rev. Lett. **57**, 1899 (1986).
[30]D. Pfirsch and D. Correa-Restrepo, Plasma Phys. Controlled Fusion **38**, 71 (1996).
[31]B. Scott, in *Europhysics Conference Abstracts, Proceedings of the 22nd European Physical Society Conference on Controlled Fusion and Plasma Physics*, Bournemouth, 1995, edited by B. E. Keen, P. E. Stott, and J. Winter (European Physical Society, Petit-Lancy, 1995), Vol. 19C, p. I-231.
[32]N. Mattor and P. H. Diamond, Phys. Plasmas **1**, 4002 (1994); N. Mattor, *ibid*. **2**, 766 (1995).
[33]S. Raycharedhuri, Nucl. Fusion **35**, 1281 (1995).
[34]A. Zeiler, D. Biskamp, J. F. Drake, and P. N. Guzdar, ''3D fluid simulations of tokamak edge turbulence,'' submitted to Phys. Plasmas.
[35]A. Hasegawa and M. Wakatani, Phys. Rev. Lett. **50**, 682 (1985).
[36]S. J. Camargo, D. Biskamp, and B. D. Scott, Phys. Plasmas **2**, 48 (1995).
[37]A. E. Koniges, J. A. Crotinger, and P. H. Diamond, Phys. Fluids B **4**, 2785 (1992).
[38]F. Y. Gang, B. D. Scott, and P. H. Diamond, Phys. Fluids B **1**, 1331 (1989).
[39]X. Q. Xu, R. H. Cohen, J. A. Crotinger, and A. I. Shestakov, Phys. Plasmas **2** (1995).
[40]D. Biskamp and A. Zeiler, Phys. Rev. Lett. **74**, 706 (1995).
[41]A. Hasegawa and M. Wakatani, Phys. Fluids **26**, 2770 (1983).
[42]R. D. Hazeltine, Phys. Fluids **26**, 3242 (1983).
[43]J. F. Drake, T. M. Antonsen, Jr., A. B. Hassam, and N. T. Gladd, Phys. Fluids **26**, 2509 (1983).
[44]Isothermal: B. D. Scott, A. B. Hassam, and J. F. Drake, Phys. Fluids **28**, 275 (1985); with temperature: B. D. Scott and A. B. Hassam, *ibid*. **30**, 90 (1987).
[45]N. Bekki and Y. Kaneda, Phys. Rev. Lett. **57**, 2176 (1986).
[46]B. Scott, in *Europhysics Conference Abstracts, Proceedings of the 21st EPS Conference on Controlled Fusion and Plasma Physics*, Montpellier, 1994, edited by E. Joffrin, P. Platz, and P. E. Stott (European Physical Society, Petit-Lancy, 1994), Vol. 18B, p. II-560.
[47]B. D. Scott, J. Comput. Phys. **78**, 114 (1988).
[48]J. F. Drake and A. B. Hassam, Phys. Fluids **24**, 1262 (1981).
[49]Isothermal: B. D. Scott, H. Biglari, P. W. Terry, and P. H. Diamond, Phys. Fluids B **3**, 51 (1991); with temperature: B. D. Scott, *ibid*. **4**, 2468 (1992).
[50]B. D. Scott, Nucl. Fusion **32**, 873 (1992).
[51]S. I. Braginskii, in *Reviews of Plasma Physics*, edited by M. A. Leontovich (Consultants Bureau, New York, 1965), Vol. 1, p. 205.
[52]J. A. Domaradzski, Phys. Fluids **31**, 2747 (1988).